Hard-core lattice model of multiphase systems

H. P. Neumann
Institut für Physikalische Chemie der Universität Frankfurt/Main, Frankfurt-am-Main, Germany
(Received 21 November 1974)

The cooperative-problem lattice model for gases, liquids, and solids on a face-centered-cubic lattice is approximately solved. A hard-core interaction is assumed between particles on nearest-, next-nearest-, and on next-but-one nearest-neighbor lattice sites. Particles on lattice sites which are at a greater distance from one another are connected by an arbitrary soft pair interaction whose zero Fourier component may be positive or negative. By considering not only homogeneous particle distributions but also some simple periodical particle distributions on the lattice we can, in the case of a mean attractive soft particle interaction, prove the possibility of the existence of four thermodynamical stable phases: a gas phase, a liquid phase, a solid modification with a face-centered-cubic periodical structure, and a solid modification with a simple cubic periodical structure. Transitions between these phases can take place.

I. INTRODUCTION

A general statistical thermodynamical theory which predicts all possible phases of a classical many-particle model of a real substance and describes the thermodynamical behavior of all these phases completely if a definite particle interaction is given, is still not available. The reason is the great mathematical difficulty of evaluating the grand canonical partition function. Nevertheless, the possibility of the existence of several different equilibrium particle density distributions, corresponding to different thermodynamically stable phases, could be proved within the frame of simple lattice models. Although these models are in many cases not completely true-to-nature pictures, they allow us to understand, in principle, how the interaction between the microscopical parts of a real substance influences its macroscopically thermodynamical behavior. On the basis of these models and with comparatively little mathematical work, one can calculate phase diagrams which are at least qualitatively in good agreement with experimental results.[38]

Examples which have been treated up to the present are (a) the Ising lattice-gas models for a gas-liquid system,[1-3] (b) the pure hard-core compound lattice models of a two-phase fluid-solid system,[8-26] and (c) the extended hard-core compound lattice models with an added soft particle interaction describing fluid-solid systems which can occur in a maximum of three phases.[27-34,39,43-45]

Recently, some comparatively simple lattice models with competing short-range repulsive and long-range attractive particle interactions have been studied. These appear to exhibit the thermodynamical behavior of a system with more than three phases.[40-42]

The present paper investigates an extended hard-core compound lattice model which, like the other models,[40-42] is still not a completely true picture of realistic multiphase systems in nature, but exhibits characteristic features of the thermodynamical behavior of certain systems. Examples in nature are the three-phase systems of inert gases and the four-phase system of sulfur. A section of the compound lattice of this model is shown in Fig. 1.

The compound lattice is a face-centered-cubic (fcc) lattice, built up by V lattice sites, which is composed of black and hatched fcc sublattices and a white complementary sublattice. The black and the hatched sublattices, which may be designated 1 and 3, respectively, consist of g_1V and g_3V lattice sites with $g_1 = g_3 = \frac{1}{8}$. The white sublattice, designated 2, consists of g_2V lattice sites with

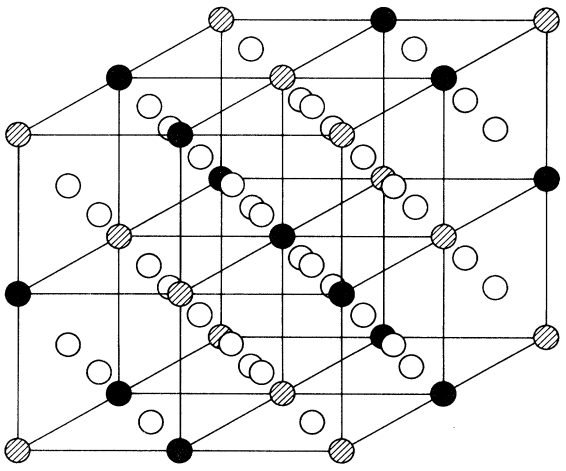

FIG. 1. Face-centered-cubic compound lattice composed of three sublattices.

$g_2 = \frac{6}{8}$.

With the aid of a compound lattice like that in Fig. 1, a greater number of phases of different geometrical and physical structures can be simulated in principle. If one considers a statistical ensemble of lattices, one can imagine homogeneous particle density distributions $\rho_\nu = N_\nu / g_\nu V$ on the three sublattices of our compound lattice model ($\nu = 1, 2, 3$; N_ν is the number of particles on the sublattice ν). With the aid of these sublattice densities ρ_ν, the following statistical homogeneous or periodical particle density distributions over the whole fcc lattice can be generated in principle:

I. $\rho_1 > \rho_2 > \rho_3$, $\rho_1 \equiv \rho_3 > \rho_2$,

$\rho_1 \equiv \rho_2 \equiv \rho_3$;

II. $\rho_2 > \rho_1 > \rho_3$, $\rho_1 > \rho_3 \equiv \rho_2$,

$\rho_2 \equiv \rho_1 > \rho_3$, $\rho_2 > \rho_1 \equiv \rho_3$,

$\rho_1 > \rho_3 > \rho_2$.

It will be shown from the state equations to be derived later that density distributions represented by I can, within the frame of our approximation, be interpreted partially as equilibrium distributions of the lattice model which belong to certain stable phases. The structure $\rho_1 > \rho_2 > \rho_3$ may then be considered as a solid phase with fcc structure, and will be called the *solid phase*. The structure $\rho_1 \equiv \rho_3 > \rho_2$ may then be considered as a strongly distorted crystal (or an ordered crystalline liquid) of simple cubic symmetry. It will be called the *modification*. $\rho_1 \equiv \rho_2 \equiv \rho_3$ can represent fluid phases of various densities. In our model, only two fluid phases will occur: one fluid phase which is stable at higher densities, which will be called *liquid*, and one fluid phase that is stable at lower densities, which will be called *gas*. These are the four phases of our model.

The density distributions II will not result as a reasonable solution from the approximated state equations (6), (13), and (21)–(25) which belong to stable phases of the model. They are therefore of no physical interest.

Some assumptions about the particle interaction must be made to complete the construction of the model. The interaction may be a two-body interaction $-v_{ij}$ consisting of the following.

(i) *An extended hard core with* $v_{ij} = -\infty$ for $i = j$ and for pairs (i, j) of nearest-, next-nearest-, and next-but-one nearest-neighbor lattice sites.

(ii) *A soft interaction tail characterized by the following properties:* For all other pairs of lattice sites [which are not counted in (i)], v_{ij} may be an arbitrary regular function of the lattice site distance $|i - j|$ which is summable in the sense that the restricted sums

$$v(r) = \sum_j^{(r)} v_{ij}, \quad v(rs) = \sum_j^{(r,s)} v_{ij}, \qquad r, s = 1, 2, 3 \quad (1)$$

exist. The sums are restricted in that $i = j$ and the pairs considered in (i) are forbidden. In $v(r)$, the fixed index i designates an arbitrary lattice site of the sublattice r, and the running index j designates all the other sites of the same sublattice r which are not forbidden by the restriction. $v(r)$ represents the negative potential energy of sublattice r per lattice site. The fixed index i in $v(rs)$ designates an arbitrary lattice site of sublattice r, while the running index j covers all lattice sites of the other sublattice s which are not forbidden by the restriction. $v(rs)$ represents the negative potential energy per lattice site of sublattice r with sublattice s.

The following symmetry relations are valid between the $v(r)$ and $v(rs)$:

$$\begin{aligned} &v(1) = v(3), \quad v(13) = v(31), \\ &v(12) = v(32), \quad v(12) = (g_2/g_1)\, v(21), \\ &v(21) = v(23). \end{aligned} \quad (2)$$

With the aid of the $v(r)$ and $v(rs)$, the total negative interaction energy per lattice site on the whole lattice $-v$ is given by

$$v = v(r) + \sum_{s=1, s\neq r}^{3} v(rs), \quad r = 1, 2, 3. \quad (3)$$

Apart from the strengths of the interaction v, the geometrical structure of the interaction plays an important role in the attempt to clarify the connection between particle interaction structure and phase transition behavior of the model by the theory. In the frame of our theory, it is useful to characterize the interaction structure by the following two interaction structure parameters $\bar{v}(12)$ and $\bar{v}(13)$:

$$\begin{aligned} \bar{v}(12) &= \frac{v(1) + v(13) - 2v(21)}{v} = \frac{v(2) - v(12)}{v}, \\ \bar{v}(13) &= \frac{v(1) - v(31)}{v} = \frac{v(3) - v(13)}{v}. \end{aligned} \quad (4)$$

$v(r)$ and $v(rs)$ are completely determined by v, $\bar{v}(12)$, and $\bar{v}(13)$ according to

$$\begin{aligned} v(1) &= g_1 v[1 + 3\bar{v}(12) + 4\bar{v}(13)], \\ v(2) &= g_2 v[3 + \bar{v}(12)], \\ v(13) &= g_1 v[1 + 3\bar{v}(12) - 4\bar{v}(13)], \\ v(12) &= g_2 v[1 - \bar{v}(12)]. \end{aligned} \quad (5)$$

The grand canonical partition function Ξ of the model defined above can now be evaluated in mean-field approximation.[43-45] The result is a comparatively simple relation between the pressure p, the temperature T, the sublattice densities ρ_ν, and the chemical potential μ of the model on the one hand, and the interaction terms $v(r)$ and $v(rs)$ on the other hand:

$$p = \tfrac{1}{2}[\, g_1 v(1)(\rho_1)^2 + g_3 v(3)(\rho_3)^2 + g_2 v(2)(\rho_2)^2 + g_1 v(12)\rho_1\rho_2 + g_2 v(21)\rho_2\rho_1 + g_1 v(13)\rho_1\rho_3 + g_3 v(31)\rho_3\rho_1 + g_2 v(23)\rho_2\rho_3 + g_3 v(32)\rho_3\rho_2 + 2(g_1\rho_1 + g_3\rho_3 + g_2\rho_2)\mu] + (1/V\beta)\ln[W_{hc}(\rho_1,\rho_2,\rho_3)]. \quad (6)$$

$W_{hc}(\rho_1,\rho_2,\rho_3)$ in (6) is the so-called combinatorial factor of Ξ, that is, the number of all configurations on the lattice with fixed sublattice densities ρ_1,ρ_2,ρ_3 which are compatible with the hard-core interaction. β is the conventional abbreviation $\beta = 1/kT$ with k the Boltzmann constant. The formula (6) is only of practical use if $W_{hc}(\rho_1,\rho_2,\rho_3)$ can be evaluated. This will be done approximately in Sec. II.

The derivation of state equations on the basis of (6), their solution and the construction of corresponding state and phase diagrams will follow in the other sections.

II. EVALUATION OF THE COMBINATORIAL FACTOR $W_{hc}(\rho_1,\rho_2,\rho_3)$

The calculation of combinatorial factors is a central problem in statistical mechanics. The difficulty in our case is correct consideration of the hard-core correlation. The hard-core correlation of our model is transferred by a limited set of subfigures. These subfigures are all differently occupied (by a maximum of one particle because of the hard-core interaction) or empty lattice site subsets. The largest subsets, the so-called basic subsets, are the sets 8a–8d in Fig. 2.

Figure 2 shows further subsets which together with 8a–8d form a so-called overlapping sequence. This means that each member is generated by an overlapping of two members which precede it in the sequence. The subsets in Fig. 2 are designated by a double index lh, where l is the number of lattice sites and h the type of the subset. In our model, a transfer of the hard-core correlation may be approximately considered only by the subfigures formed of (single-particle) occupied or empty subsets of the types shown in Fig. 2.

The state of occupation of a subset lh with one particle may be designated by an index k which assumes the values $0, 1, 2, 3$. $k=0$ designates the empty state. $k=1$ denotes the occupation of a black site of sublattice 1. $k=2$ denotes the occupation of a white lattice site of sublattice 2. $k=3$ denotes the occupation of a hatched lattice site of sublattice 3. In this way, a subfigure is not uniquely but sufficiently characterized by the indices lh and k. (A complete designation indicating which single lattice site is occupied remains open.) Consider once again a statistical lattice ensemble on which the particles are distributed with sublattice densities ρ_1,ρ_2,ρ_3: there is then also a distribution of the subfigures with indices (lh,k) mentioned above with corresponding mean occupation numbers or probabilities. These distribution probabilities may be designated $\langle p^{(lh)}\rangle(k)$ [$\langle p^{(lh)}\rangle(k)$ is the number of subfigures lh,k divided by the number of subsets lh].

For reasons of consistency, the $\langle p^{(lh)}\rangle(k)$ are only functions of ρ_k. These functions are summarized in Table I. Probabilities $\langle p^{(lh)}\rangle(k)$ of subfigures lh,k, which differ only in that different sites of the same sublattice are occupied, are equal. This means that $\langle p^{(lh)}\rangle(k)$ occurs with a multiplicity $j(lh,k)$. For example, because the subsets 8a–8d each have six white lattice sites, there are $j(8h,2)=6$ different subfigures for each

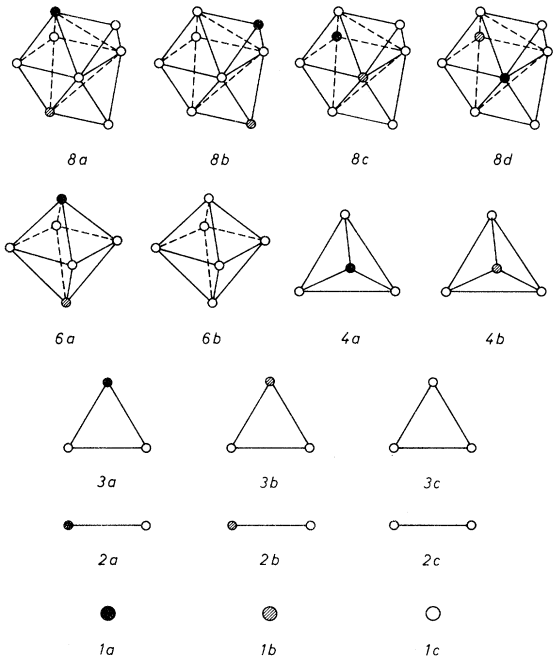

FIG. 2. An overlapping sequence of lattice site subsets lh which participate in the transfer of the hard-core correlation.

TABLE I. Subfigure probabilities $\langle p^{(lh)}\rangle(k)$ and coefficients of multiplicity $j(lh,k)$.

	$\langle p^{(lh)}\rangle(1)$	$j(lh,1)$	$\langle p^{(lh)}\rangle(2)$	$j(lh,2)$	$\langle p^{(lh)}\rangle(3)$	$j(lh,3)$	$\langle p^{(lh)}\rangle(0)$	$j(lh,0)$
8a								
8b	ρ_1	1		6	ρ_3	1	$1-\rho_1-\rho_3-6\rho_2$	
8c								
8d								
6a	ρ_1	1		4	ρ_3	1	$1-\rho_1-\rho_3-4\rho_2$	
6b	0	0	ρ_2	6	0	0	$1-6\rho_2$	1
4a	ρ_1	1		3	0	0	$1-\rho_1-3\rho_2$	
4b	0	0			ρ_3	1	$1-\rho_3-3\rho_2$	
3a	ρ_1	1		2	0		$1-\rho_1-2\rho_2$	
3b	0	0			ρ_3	1	$1-\rho_3-2\rho_2$	
3c				3	0		$1-3\rho_2$	
2a	ρ_1	1		1	0	0	$1-\rho_1-\rho_2$	
2b	0	0		1	ρ_3	1	$1-\rho_3-\rho_2$	
2c			ρ_2	2	0	0	$1-2\rho_2$	1
1a	ρ_1	1		0	0	0	$1-\rho_1$	
1b	0	0		0	ρ_3	1	$1-\rho_3$	
1c				1	0	0	$1-\rho_2$	

subset where one white site 2 is occupied. All these subfigures are distributed with the same probability $\langle p^{(8h)}\rangle(2)=\rho_2$. The coefficients of multiplicity $j(lh,k)$ are also listed in Table I. It is now clear why the designation of a subfigure with the indices lh and k is sufficient.

The calculation of $W_{\rm hc}(\rho_1,\rho_2,\rho_3)$ in our approximation is therefore equivalent to the counting of all configurations with fixed sublattice densities ρ_k and fixed probabilities $\langle p^{(lh)}\rangle(k)$, whereby the relations of Table I between the $\langle p^{(lh)}\rangle(k)$ and ρ_k must be used. Similar problems[35-37,44,45] were treated with a method which is based on a reduction of the problem of counting configurations on the original lattice (the so-called basic lattice) to the counting of configurations on so-called pseudolattices where the correlation is limited to small ranges. Examples of pseudolattices are given in Refs. 35–37, 44, and 45 (see, e.g., Figs. 4 and 5 in Ref. 45). The pseudolattices are produced from the basic lattice by a successive decomposition into subsets belonging to an overlapping sequence (in the case of our model, the subsets of Fig. 2). Utilizing the designations given in a former paper,[45] the basic lattice may be designated $p(0)$ and the pseudolattices $p(0,l_1,-,l_n)$. $p(0,l_1,-,l_n)$ means that the basic lattice $p(0)$ is decomposed into subsets of types l_1h in a first step, delivering a pseudolattice $p(0,l_1)$. A further decomposition of the subsets l_1h of the pseudolattice $p(0,l_1)$ into subsets of types l_2h ($l_1>l_2$) delivers a pseudolattice $p(0,l_1,l_2)$. The procedure can be continued until a decomposition of the basic lattice $p(0)$ into subsets of types l_nh is reached.[45] There are many possibilities of successive decomposition. Each such successive decomposition designates a path of decomposition. The paths of decomposition of our model are listed in Table II.

On the basic lattice $p(0)$ and on each pseudolattice $p(0,l_1,-,l_n)$, there are well-defined numbers of subsets of all possible types l_mh ($l_m\leq l_n$). Instead of these numbers, densities (i.e., numbers of subsets per lattice site if V lattice sites of the basic lattice are given) can be defined. $x(0,l_1,-,l_n;l_nh)$ is the number of subsets of types l_nh per lattice site on the pseudolattice $p(0,l_1,-,l_n)$. In Table III, the $x(0,l_1,-,l_n;l_nh)$ are stated as functions of the coordination number z of the basic lattice ($z=12$) and the lattice site densities g_ν for all pseudolattices considered in Table II. In Tables II and III some pseudolattices are designated as $p(0,l_1,\ldots,6\text{–}4,\ldots,l_n)$. This means that a simultaneous decomposition in subsets of types $6h$ and $4h$ is performed in one step only.

On a pseudolattice $p(0,l_1,-,l_n)$ one can—as for the basic lattice $p(0)$—also consider distribution

TABLE II. A scheme of the various possibilities of a decomposition of the basic lattice into a series of pseudolattices. Path I = complete decomposition. Paths II, III, IV = decompositions where one, two and three pseudolattices have been dropped in the series of decomposition. Path V = direct decomposition.

I		$p(0) \rightarrow p(0,8) \rightarrow p(0,8,6-4) \rightarrow p(0,8,6-4,3) \rightarrow p(0,8,6-4,3,2) \rightarrow p(0,8,6-4,3,2,1)$
II	1	$p(0) \rightarrow p(0,8) \rightarrow p(0,8,6-4) \rightarrow p(0,8,6-4,3) \rightarrow p(0,8,6-4,3,1)$
	2	$p(0) \rightarrow p(0,8) \rightarrow p(0,8,6-4) \rightarrow p(0,8,6-4,2) \rightarrow p(0,8,6-4,2,1)$
	3	$p(0) \rightarrow p(0,8) \rightarrow p(0,8,3) \rightarrow p(0,8,3,2) \rightarrow p(0,8,3,2,1)$
	4	$p(0) \rightarrow p(0,6-4) \rightarrow p(0,6-4,3) \rightarrow p(0,6-4,3,2) \rightarrow p(0,6-4,3,2,1)$
III	1	$p(0) \rightarrow p(0,8) \rightarrow p(0,8,6-4) \rightarrow p(0,8,6-4,1)$
	2	$p(0) \rightarrow p(0,8) \rightarrow p(0,8,3) \rightarrow p(0,8,3,1)$
	3	$p(0) \rightarrow p(0,8) \rightarrow p(0,8,2) \rightarrow p(0,8,2,1)$
	4	$p(0) \rightarrow p(0,6-4) \rightarrow p(0,6-4,3) \rightarrow p(0,6-4,3,1)$
	5	$p(0) \rightarrow p(0,6-4) \rightarrow p(0,6-4,2) \rightarrow p(0,6-4,2,1)$
	6	$p(0) \rightarrow p(0,3) \rightarrow p(0,3,2) \rightarrow p(0,3,2,1)$
IV	1	$p(0) \rightarrow p(0,8) \rightarrow p(0,8,1)$
	2	$p(0) \rightarrow p(0,6-4) \rightarrow p(0,6-4,1)$
	3	$p(0) \rightarrow p(0,3) \rightarrow p(0,3,1)$
	4	$p(0) \rightarrow p(0,2) \rightarrow p(0,2,1)$
V		$p(0) \rightarrow p(0,1)$

TABLE III. Subset densities $x(0,l_1,-,l_n;l_nh)$ on the pseudolattices $p(0,l_1,-,l_n)$. The first subcolumns belonging to the columns $p(0,8,6-4)$ and $p(0,6-4)$ represent the densities of the subsets 6a and 6b, while the second subcolumns represent the densities of the subsets 4a and 4b.

$p(0,l_1,-,l_n)$	$p(0,8)$	$p(0,8,6-4)$	$p(0,8,6-4,3)$	$p(0,8,6-4,3,2)$	$p(0,8,6-4,3,2,1)$	$p(0,8,6-4,3,1)$
$x(0,l_1,-,l_n;l_na)$	$2zg_1$	$6zg_1$ $8zg_1$	$4z^2g_1$	$8z^2g_1$	$8z^2g_1$	$4z^2g_1$
$x(0,l_1,-,l_n;l_nb)$	$2zg_1$	$2zg_1$ $8zg_1$	$4z^2g_1$	$8z^2g_1$	$8z^2g_1$	$4z^2g_1$
$x(0,l_1,-,l_n;l_nc)$	$2zg_1$	0	$2(z+4)zg_1$	$16z^2g_1$	$8z^2g_2$	$4z^2g_2$
$x(0,l_1,-,l_n;l_nd)$	$2zg_1$	0	0	0	0	0
$p(0,l_1,-,l_n)$	$p(0,8,6-4,2)$	$p(0,8,6-4,2,1)$	$p(0,8,6-4,1)$	$p(0,8,3)$	$p(0,8,3,2)$	$p(0,8,3,2,1)$
$x(0,l_1,-,l_n;l_na)$	$4z^2g_1$	$4z^2g_1$	$(z+2)zg_1$	$3z^2g_1$	$6z^2g_1$	$6z^2g_1$
$x(0,l_1,-,l_n;l_nb)$	$4z^2g_1$	$4z^2g_1$	$(z+2)zg_1$	$3z^2g_1$	$6z^2g_1$	$6z^2g_1$
$x(0,l_1,-,l_n;l_nc)$	$8z^2g_1$	$4z^2g_2$	$(z+2)zg_2$	$2z^2g_1$	$12z^2g_1$	$6z^2g_2$
$p(0,l_1,-,l_n)$	$p(0,8,3,1)$	$p(0,8,2)$	$p(0,8,2,1)$	$p(0,8,1)$	$p(0,6-4)$	$p(0,6-4,3)$
$x(0,l_1,-,l_n;l_na)$	$3z^2g_1$	$3z^2g_1$	$3z^2g_1$	$8zg_1$	$\frac{1}{2}zg_1$ $\frac{2}{3}zg_1$	$4zg_1$
$x(0,l_1,-,l_n;l_nb)$	$3z^2g_1$	$3z^2g_1$	$3z^2g_1$	$8zg_1$	$\frac{1}{6}zg_1$ $\frac{2}{3}zg_1$	$4zg_1$
$x(0,l_1,-,l_n;l_nc)$	$3z^2g_2$	$6z^2g_1$	$3z^2g_2$	$8zg_2$	0	$\frac{8}{3}zg_1$
$p(0,l_1,-,l_n)$	$p(0,6-4,3,2)$	$p(0,6-4,3,2,1)$	$p(0,6-4,3,1)$	$p(0,6-4,2)$	$p(0,6-4,2,1)$	$p(0,6-4,1)$
$x(0,l_1,-,l_n;l_na)$	$8zg_1$	$8zg_1$	$4zg_1$	$4zg_1$	$4zg_1$	$\frac{7}{6}zg_1$
$x(0,l_1,-,l_n;l_nb)$	$8zg_1$	$8zg_1$	$4zg_1$	$4zg_1$	$4zg_1$	$\frac{7}{6}zg_1$
$x(0,l_1,-,l_n;l_nc)$	$z(z+4)g_1$	$8zg_2$	$4zg_2$	$8zg_1$	$4zg_2$	$\frac{7}{6}zg_2$
$p(0,l_1,-,l_n)$	$p(0,3)$	$p(0,3,2)$	$p(0,3,2,1)$	$p(0,3,1)$	$p(0,2)$	$p(0,2,1)$ $p(0,1)$
$x(0,l_1,-,l_n;l_na)$	$2zg_1$	$4zg_1$	$4zg_1$	$2zg_1$	zg_1	zg_1 g_1
$x(0,l_1,-,l_n;l_nb)$	$2zg_1$	$4zg_1$	$4zg_1$	$2zg_1$	zg_1	zg_1 g_1
$x(0,l_1,-,l_n;l_nc)$	$\frac{4}{3}zg_1$	$8zg_1$	$4zg_2$	$2zg_2$	$2zg_1$	zg_2 g_2

probabilities $\langle p^{(l_m h)}\rangle(k)$ of all possible subfigures with $l_m \leq l_n$. One can then ask for the number $Q(0, l_1, -, l_n; \langle p^{(l_m h)}\rangle(k))$ of configurations on the pseudolattice $p(0, l_1, -, l_n)$ or the basic lattice $p(0)$ with fixed probabilities $\langle p^{(l_m h)}\rangle(k)$ $(l_m \leq l_n)$. The configuration numbers $Q(0, l_1, -, l_n; \langle p^{(l_m h)}\rangle(k))$ increase if one proceeds along a path of decomposition in Table II, because the restrictions imposed on the configurations are eliminated one by one as the range of correlation is successively reduced and disconnection of the lattice grows.

The counting of the $Q(0, l_1, -, l_n; \langle p^{(l_m h)}\rangle(k))$ however remains a difficult problem if $l_n \neq l_m$. It therefore appears reasonable to try an approximation of $W_{hc}(\rho_1, \rho_2, \rho_3)$ by a simple function of the $Q(0, l_1, -, l_n; \langle p^{(l_m h)}\rangle(k))$ with $l_m = l_n$. These configuration numbers can be easily calculated by the formula

$$Q(0, l_1, -, l_n; \langle p^{(l_n h)}\rangle(k)) = \prod_{l_n h} \frac{[x(0, l_1, -, l_n; l_n h)V]!}{\prod_{k=0}^{3}\{[\langle p^{(l_n h)}\rangle(k)\, x(0, l_1, -, l_n; l_n h)V]!\}^{j(l_n h, k)}}. \tag{7}$$

In the case of the pseudolattices $p(0, l_1, -, 6\text{–}4)$ the product index $l_n h$ in (7) assumes the values 6a, 6b, 4a, 4b. In all other cases, it is simply $l_n a, l_n b, \ldots$.

A comparatively simple functional dependence of $W_{hc}(\rho_1, \rho_2, \rho_3)$ from the Q's of (7) can be found with the aid of the following set of combinatorial Ansätze:

$$\frac{Q(0, l_1, -, l_m; \langle p^{(l_n h)}\rangle(k))}{Q(0, l_1, -, l_m, l_n; \langle p^{(l_n h)}\rangle(k))} = \Gamma(0, l_1, -, l_m | 0, l_1, -, l_m, l_n; l_n), \tag{8}$$

$$\frac{Q(0, l_1, -, l_m; \langle p^{(l_n' h)}\rangle(k))}{Q(0, l_1, -, l_m, l_n; \langle p^{(l_n' h)}\rangle(k))} = \Gamma(0, l_1, -, l_m | 0, l_1, -, l_m, l_n; l_n'), \tag{9}$$

$$\Gamma(0, l_1, -, l_m | 0, l_1, -, l_m, l_n; l_n) = [\Gamma(0, l_1, -, l_m | 0, l_1, -, l_m, l_n; l_n')]^{\alpha(0, l_1, -, l_m, l_n)}, \tag{10}$$

$$W_{hc}(\rho_1, \rho_2, \rho_3) = Q(0; \langle p^{(8h)}\rangle(k)). \tag{11}$$

The $\alpha(0, l_1, -, l_m, l_n)$ in (10) are arbitrary positive functions of the sublattice densities ρ_ν. There are 15 relations (10). The corresponding index sets

$$l_1, -, l_m | l_1, -, l_m, l_n; l_n$$

and

$$l_1, -, l_m | l_1, -, l_m, l_n; l_n'$$

are listed in Table IV.

The system of equations (8)–(11) allows now an elimination of the $Q(0, l_1, -, l_n; \langle p^{(l_m h)}\rangle(k))$ with $l_m \neq l_n$ which are not easily calculable functions of the probabilities $\langle p^{(l_m h)}\rangle(k)$. The result is a simple rational function

$$W_{hc}(\rho_1, \rho_2, \rho_3) = \Omega\{[Q(0, l_1, -, l_n; \langle p^{(l_n h)}\rangle(k))]\}, \tag{12}$$

whereby all Q's of the system (8)–(11), calculable according to (7), occur in (12). If one uses the density functions $\langle p^{(lh)}\rangle(k)$ listed in Table I and also Stirling's formula for great values of V in (7), (12) can be easily evaluated, delivering

$$\begin{aligned}(1/V)\ln[W_{hc}(\rho_1, \rho_2, \rho_3)] = {} & -g_1\delta\rho_1 \ln\rho_1 - g_3\delta\rho_3 \ln\rho_3 - g_2\delta\rho_2 \ln\rho_2 + g_1\gamma(1-\rho_1)\ln(1-\rho_1) \\ & + g_3\gamma(1-\rho_3)\ln(1-\rho_3) + g_2\gamma(1-\rho_2)\ln(1-\rho_2) + g_1\epsilon(1-\rho_1-\rho_2)\ln(1-\rho_1-\rho_2) \\ & + g_3\epsilon(1-\rho_3-\rho_2)\ln(1-\rho_3-\rho_2) + g_2 2(g_1/g_2)\epsilon(1-2\rho_2)\ln(1-2\rho_2) \\ & + g_1\varphi(1-\rho_1-2\rho_2)\ln(1-\rho_1-2\rho_2) + g_3\varphi(1-\rho_3-2\rho_2)\ln(1-\rho_3-2\rho_2) \\ & + g_2\tfrac{2}{3}(g_1/g_2)\varphi(1-3\rho_2)\ln(1-3\rho_2) + g_1\psi(1-\rho_1-3\rho_2)\ln(1-\rho_1-3\rho_2) \\ & + g_3\psi(1-\rho_3-3\rho_2)\ln(1-\rho_3-3\rho_2) + g_1\chi(1-\rho_1-\rho_3-4\rho_2)\ln(1-\rho_1-\rho_3-4\rho_2) \\ & + g_1 2(g_1/g_2)\chi[1-(g_2/g_1)\rho_2]\ln[1-(g_2/g_1)\rho_2] \\ & - g_1 8z[1-\rho_1-\rho_3-(g_2/g_1)\rho_2]\ln[1-\rho_1-\rho_3-(g_2/g_1)\rho_2],\end{aligned} \tag{13}$$

whereby $\gamma, \delta, \epsilon, \varphi, \psi, \chi$ are the following functions of the α's from (10):

$$\delta = \alpha(0,2)\alpha(0,3)\alpha(0,6-4) + z\{8 + \alpha(0,8)[-\tfrac{77}{6} + \alpha(0,6-4)\{-2 + \alpha(0,3)[-3 - \alpha(0,2) + 2\alpha(0,3,2)] + \alpha(0,6-4,3)[4 + 4\alpha(0,6-4,3,2) + \tfrac{17}{6}\alpha(0,6-4,2)] - 8\alpha(0,6-4,2)\alpha(0,6-4,3,2)\} + \alpha(0,8,6-4)(-8\alpha(0,8,2)\alpha(0,8,3) + z\{1 + 3\alpha(0,8,3)[1 + \alpha(0,8,2) - \alpha(0,8,3,2)]\})]\}, \tag{14}$$

$$\gamma = -\alpha(0,2)\alpha(0,3)\alpha(0,6-4) + z\,\alpha(0,8)(\alpha(0,6-4)\{\alpha(0,3)[\alpha(0,2) - 2\alpha(0,3,2)] + \alpha(0,6-4,3)[-4\alpha(0,6-4,3,2) - \tfrac{17}{6}\alpha(0,6-4,2)] + 8\alpha(0,6-4,2)\alpha(0,6-4,3,2)\} + \alpha(0,8,6-4)\{8\alpha(0,8,3)\alpha(0,8,2) - 3z\,\alpha(0,8,3)[\alpha(0,8,2) - \alpha(0,8,3,2)]\}), \tag{15}$$

$$\epsilon = z\,\alpha(0,8)\{\alpha(0,6-4)[3\alpha(0,3) - 4\alpha(0,6-4,3)] - 3z\,\alpha(0,8,3)\alpha(0,8,6-4)\}, \tag{16}$$

$$\varphi = z\,\alpha(0,8)[2\alpha(0,6-4) - z\,\alpha(0,8,6-4)], \tag{17}$$

$$\psi = \tfrac{22}{3} z\,\alpha(0,8), \tag{18}$$

$$\chi = \tfrac{3}{4}\psi = \tfrac{11}{2} z\,\alpha(0,8), \tag{19}$$

and z is the coordination number of the fcc lattice. The functions $\gamma, \delta, \epsilon, \varphi, \psi, \chi$ are not independent, but are restricted apart from (19) by the relation

$$\delta + \gamma + \epsilon + \varphi + \psi + \chi = 8z. \tag{20}$$

The formula (13) for $W_{hc}(\rho_1, \rho_2, \rho_3)$ can even be correct if the α functions from (10) are correspondingly chosen.

Because the α functions influence $W_{hc}(\rho_1, \rho_2, \rho_3)$ only over the functions $\gamma, \delta, \epsilon, \varphi, \psi, \chi$ from (14)–(19), there are many possibilities for a suitable choice of the α functions.

A simple ansatz can be obtained by the assumption that $\gamma, \delta, \epsilon, \varphi, \psi, \chi$ are very slowly varying functions of the sublattice densities ρ_ν which can be replaced by constant parameters chosen in the way that most reasonable results will be obtained. The condition $\alpha(l_1, -, l_n) > 0$ must be fulfilled thereby, of course. Combinatorial Ansätze of this kind (so-called MQC approximations) were comparatively successful in the cases of some other hard-core lattice models.[44,45] They may therefore also be used for our model.

III. STATE EQUATIONS AND THEIR SOLUTION

A complete system of mean-field state equations is obtained if $(1/V)\ln[W_{hc}(\rho_1, \rho_2, \rho_3)]$ of (13) is inserted in (6) and the sublattice densities ρ_ν are determined in the way that the resulting pressure function becomes maximum. This means that $\partial p/\partial\rho_1 = \partial p/\partial\rho_2 = \partial p/\partial\rho_3 = 0$ must be fulfilled. A differentiation of (6) combined with (13) delivers the following state equations:

$$\frac{(1-\rho_1)^\gamma(\rho_1)^\delta(1-\rho_1-\rho_2)^\epsilon(1-\rho_1-2\rho_2)^\varphi(1-\rho_1-3\rho_2)^\psi(1-\rho_1-\rho_3-4\rho_2)^\chi}{[1-\rho_1-\rho_3-(g_2/g_1)\rho_2]^{8z}} = \exp\{\beta[v(1)\rho_1 + v(12)\rho_2 + v(13)\rho_3 + \mu]\}, \tag{21}$$

$$\frac{(1-\rho_3)^\gamma(\rho_3)^\delta(1-\rho_3-\rho_2)^\epsilon(1-\rho_3-2\rho_2)^\varphi(1-\rho_3-3\rho_2)^\psi(1-\rho_1-\rho_3-4\rho_2)^\chi}{[1-\rho_1-\rho_3-(g_2/g_1)\rho_2]^{8z}} = \exp\{\beta[v(3)\rho_3 + v(32)\rho_2 + v(31)\rho_1 + \mu]\}, \tag{22}$$

$$((1-\rho_2)^\gamma(\rho_2)^\delta\{(1-\rho_1-\rho_2)^\epsilon(1-\rho_3-\rho_2)^\epsilon(1-2\rho_2)^{4\epsilon}(1-\rho_1-2\rho_2)^{2\varphi}(1-\rho_3-2\rho_2)^{2\varphi}(1-3\rho_2)^{2\varphi}(1-\rho_1-3\rho_2)^{3\psi} \times (1-\rho_3-3\rho_2)^{3\psi}(1-\rho_1-\rho_3-4\rho_2)^{4\chi}[1-(g_2/g_1)\rho_2]^{2\chi}\}^{(g_1/g_2)}/[1-\rho_1-\rho_3-(g_2/g_1)\rho_2]^{8z} = \exp\{\beta[v(2)\rho_2 + v(21)\rho_1 + v(23)\rho_3 + \mu]\}, \tag{23}$$

$$\frac{dp}{d\mu} = \rho, \tag{24}$$

$$\rho = g_1\rho_1 + g_2\rho_2 + g_3\rho_3. \tag{25}$$

The coupled system of transcendental equations (21)–(23) can be solved by a graphical method after a separation which leads to the following system of equations:

$$\lambda^{**} = (1-\rho_1)^{\gamma}(\rho_1)^{\delta}(1-\rho_1-\rho_2)^{\epsilon}(1-\rho_1-2\rho_2)^{\varphi}(1-\rho_1-3\rho_2)^{\psi}\exp[-\beta v\bar{v}(13)\rho_1], \tag{26}$$

$$\lambda^{**} = (1-\rho_3)^{\gamma}(\rho_3)^{\delta}(1-\rho_3-\rho_2)^{\epsilon}(1-\rho_3-2\rho_2)^{\varphi}(1-\rho_3-3\rho_2)^{\psi}\exp[-\beta v\bar{v}(13)\rho_3], \tag{27}$$

$$\lambda^{*} = (1-\rho_2)^{\gamma}(\rho_2)^{\delta}[(1-2\rho_2)^{4\epsilon}(1-3\rho_2)^{2\varphi}(1-(g_2/g_1)\rho_2)^{2\chi}]^{g_1/g_2}\exp[-\beta v\bar{v}(12)\rho_2], \tag{28}$$

$$\lambda = \lambda^{**}[1-(\rho_1+\rho_3)-4\rho_2]^{\chi}\exp\{\beta v[\bar{v}(13)-\bar{v}(12)](\rho_1+\rho_3)/2\}, \tag{29}$$

$$\lambda = \lambda^{*}[(1-\rho_1-\rho_2)^{\epsilon}(1-\rho_3-\rho_2)^{\epsilon}(1-\rho_1-2\rho_2)^{2\varphi}(1-\rho_3-2\rho_2)^{2\varphi}(1-\rho_1-3\rho_2)^{3\psi} \times(1-\rho_3-3\rho_2)^{3\psi}(1-\rho_1-\rho_3-4\rho_2)^{4\chi}]^{g_1/g_2}, \tag{30}$$

$$\lambda = (1-\rho/g_1)^{8\varepsilon}\exp(\beta\{v[1-\bar{v}(12)]\rho+\mu\}), \tag{31}$$

whereby the relations between the sublattice interactions and the interaction structure parameters derived in (2)–(5) are used.

On account of (29) and (30), the following relation between λ^* and λ^{**} is valid:

$$\lambda^{**} = \lambda^{*}[(1-\rho_1-\rho_2)^{\epsilon}(1-\rho_3-\rho_2)^{\epsilon}(1-\rho_1-2\rho_2)^{2\varphi}(1-\rho_3-2\rho_2)^{2\varphi}(1-\rho_1-3\rho_2)^{3\psi} \times(1-\rho_3-3\rho_2)^{3\psi}(1-\rho_1-\rho_3-4\rho_2)^{-2\chi}]^{g_1/g_2}\exp\{-\beta v[\bar{v}(13)-\bar{v}(12)](\rho_1+\rho_3)/2\}. \tag{32}$$

The graphical solution of (26)–(32) may be performed in four steps.

The *first step* is illustrated in Figs. 3 and 4. In Fig. 3(a), the functions $\lambda^{**}(\rho_1)$ and $\lambda^{**}(\rho_3)$, given by (26) and (27), respectively, are drawn for medium values of $\beta v\bar{v}(13)$ as a group of solid-line curves with group parameter ρ_2. It is now assumed that each of these curves either represents a solution $\rho_1 \equiv \rho_3$ or that two unequal sublattice density functions $\rho_1(\lambda^{**})$ and $\rho_3(\lambda^{**})$ correspond uniquely to the two branches of each curve in the interval $0 \leq \lambda^{**} \leq \lambda^{**}(P_{13})$, whereby P_{13} is the branch point.

In the last case, the median line $(\rho_1+\rho_3)/2$ for each curve is also drawn as a solid-line curve in Fig. 3(b). If $\beta v\bar{v}(13)$ increases in the positive direction, the solid-line curves in Figs. 3(a) and 3(b) are pressed against the $(\rho_1+\rho_3)/2$ axis, whereby the branch-point densities $\rho(P_{13})$ tend towards zero. If $\beta v\bar{v}(13)$ increases in the negative direction, the same curves will be stretched away from the $(\rho_1+\rho_3)/2$ axis, whereby $\rho(P_{13})$ tends towards the unit density.

The function $\lambda^*(\rho_2)$ defined by (28) exhibits a similar course to that of the solid-line curves of Fig. 3(a) in the interval $0 \leq \rho_2 \leq g_1/g_2$. The dependence on the parameter $\beta v\bar{v}(12)$ is also similar to the influence of $\beta v\bar{v}(13)$ on the group of curves in Fig. 3(a).

TABLE IV. Scheme of the index numbers $l_1,-,l_m$ and l_n,l_n' for all possible index sets $l_1,-,l_m|l_1,-,l_m,l_n;l_n$ and $l_1,-,l_m|l_1,-,l_m,l_n;l_n'$ which must be considered in connection with formulas (8)–(11).

	0	0,8	0,8	0,8	0,8,6–4
	8,6–4	6–4,3	3,2	2,1	3,2
$l_1,-,l_m$	0,8,6–4	0,8,6–4,3	0,8,3	0	0,6–4
l_n,l_n'	2,1	2,1	2,1	6–4,3	3,2
	0,6–4	0,6–4,3	0	0,3	0
	2,1	2,1	3,2	2,1	2,1

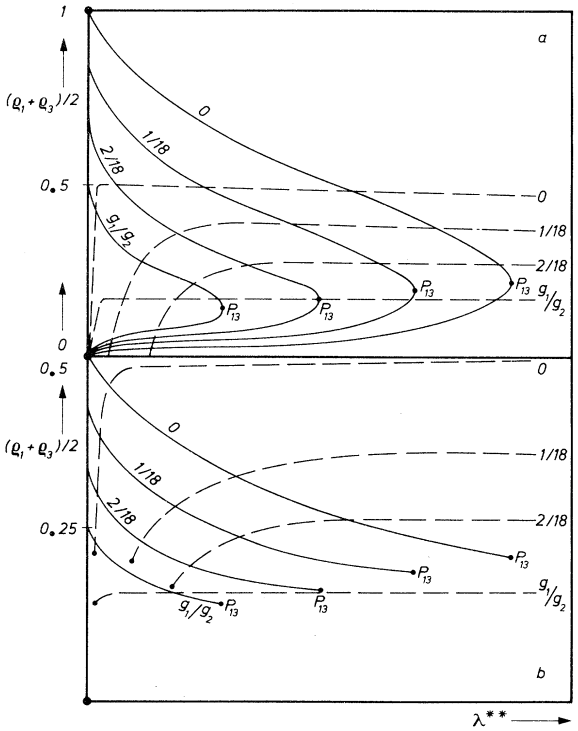

FIG. 3. Construction figure for the graphical determination of the solutions $\rho_\nu(\lambda^{**})$ ($\nu = 1, 2, 3$) of the system (26)–(28) and (32). (a) Construction of the solutions with $\rho_1 \equiv \rho_3 \neq \rho_2$ and $\rho_1 \equiv \rho_3 \equiv \rho_2$. (b) Construction of the solution with $\rho_1 \neq \rho_2 \neq \rho_3$. The numbers at the curves designate values of the group parameter ρ_2. The scale of the ordinate of (b) is doubled compared with that of (a).

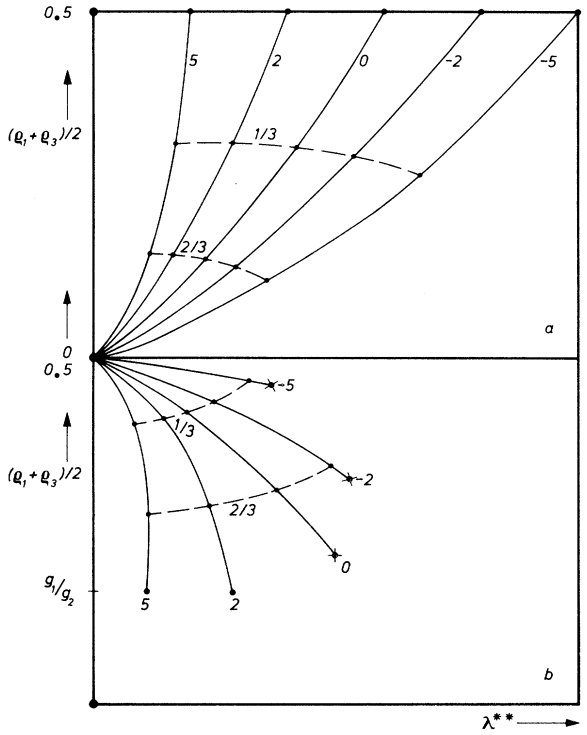

FIG. 4. Two groups of $(\rho_1+\rho_3)/2$ vs λ^{**} curves with group parameter $\beta v\bar{v}(13)$ and curve parameter ρ_2 representing solutions of (26)–(28) and (32) constructed with the aid of the method which is illustrated in Fig. 3. (a) Curves with $\rho_1 \equiv \rho_3 \neq \rho_2$. (b) Curves with $\rho_1 \neq \rho_2 \neq \rho_3$. The numbers at the solid-line curves designate values of the group parameter $\beta v\bar{v}(13)$. The numbers at the broken-line curves designate values of the curve parameter ρ_2 in units g_1/g_2 which are assumed at the intersection points of these curves with the solid-line curves. In (a) at the origin there is $\rho_2 = g_1/g_2$ while at the filled circles ●, $\rho_2 = 0$ is valid. In (b), at the point $(\rho_1+\rho_3)/2 = 0.5$, $\rho_2 = 0$ is found, while at the filled circles ●, $\rho_2 = g_1/g_2$ is valid. At the cross points ✱, values of ρ_2 with $\rho_2 < g_1/g_2$ which become smaller if $\beta v\bar{v}(13)$ decreases are assumed.

Consider now the three-dimensional $\lambda^{**}, \rho_1, \rho_3$ space: for fixed values $\beta v\bar{v}(13)$, $\beta v\bar{v}(12)$, the function (32) can be represented by a group of faces with group parameter ρ_2, because λ^* is a unique function of ρ_2 on account of (28). On the other hand, the solid-line curves of Fig. 3 can be represented by a group of space curves with group parameter ρ_2 in the $\lambda^{**}, \rho_1, \rho_3$ space. These space curves intersect the faces (32) at well-defined intersection points uniquely delivering a corresponding pair of ρ_1, ρ_3 values with $\rho_1 = \rho_3 \neq \rho_2$ for the solid-line curves of Fig. 3(a) and with $\rho_1 \neq \rho_3$ for the solid-line curves of Fig. 3(b) for each value of the group parameter ρ_2. As the space curves corresponding to Fig. 3 lie in the faces $\rho_1(\lambda^{**}), \rho_3(\lambda^{**}), \lambda^{**} = \lambda^{**}$, the same intersection points can be obtained if one intersects these curves with those curves generated by an intersection of the faces $\rho_1(\lambda^{**}), \rho_3(\lambda^{**}), \lambda^{**} = \lambda^{**}$ with the faces (32). Projections of these intersection curves with group parameter ρ_2 in the $\lambda^{**}, (\rho_1+\rho_3)/2$ plane are drawn for the case $\rho_1 \equiv \rho_3$ in Fig. 3(a) and when $\rho_1 \neq \rho_3$ in Fig. 3(b) as broken-line curves.

The intersection points of the broken-line curves with the solid-line curves in Fig. 3(a) and Fig. 3(b) are plotted correspondingly in Fig. 4(a) and Fig. 4(b) for a positive medium value of $\beta v\bar{v}(12)$ as a group of curves with group parameter $\beta v\bar{v}(13)$.

In a *second step*, the $\lambda^{**}, (\rho_1+\rho_3)/2$ curves of Fig. 4(a) and Fig. 4(b) can be mapped by the transformation (29) into the $\lambda, (\rho_1+\rho_3)/2$ plane. The result is the corresponding curves in Fig. 5(a) and Fig. 5(b). In Fig. 4 and Fig. 5, a well-defined value ρ_2 which can be considered as a curve parameter exists for every point on the curves.

In addition, it must be stated that, apart from the intersection points with $\rho_1 = \rho_3 \neq \rho_2$ in Fig. 3(a),

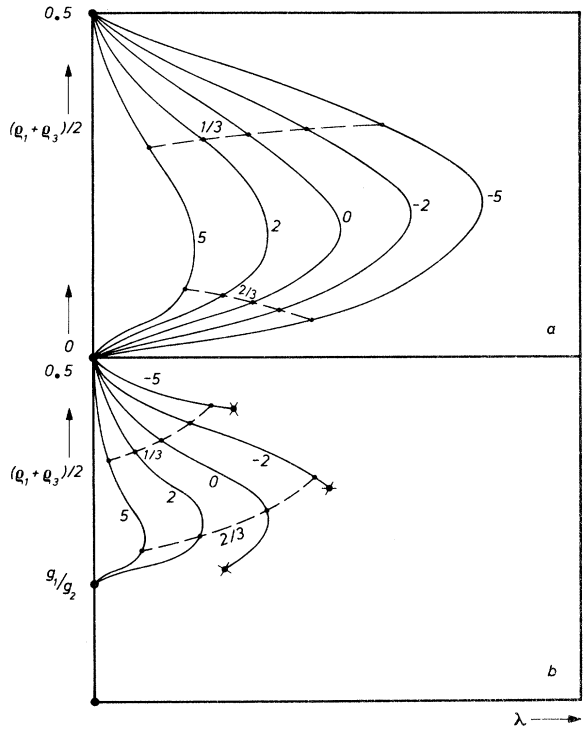

FIG. 5. Two groups of $(\rho_1+\rho_3)/2$ vs λ curves with group parameters $\beta v\bar{v}(12)$ and $\beta v\bar{v}(13)$ and curve parameter ρ_2 which are maps of the corresponding curves in Fig. 4 generated by the transformation (29). Correspondingly drawn lines and points in Fig. 5 and Fig. 4 have thereby the same meaning and belong to the same values of $\beta v\bar{v}(13)$ and ρ_2 respectively. The curves in Fig. 5(a) are independent of $\bar{v}(13)$ and vary only with group parameter $\bar{v}(12)$ while in Fig. 5(b) $\bar{v}(12)$ is kept fixed and $\bar{v}(13)$ is varied as group parameter.

there are further intersection points with $\rho_1 = \rho_3 = \rho_2$. [In every case, there are two intersection points in Fig. 3(a)!]. Corresponding curves with $\rho_1 \equiv \rho_2 \equiv \rho_3$ in Fig. 4(a) and Fig. 5(a) are however not drawn, because an analytical function

$$\lambda = (1-\rho)^{\gamma}(\rho)^{\delta}(1-2\rho)^{\epsilon}(1-3\rho)^{\varphi}(1-4\rho)^{\psi} \times [1-(g_2/g_1)\rho]^{\chi} \exp[-\beta v \bar{v}(12)\rho] \quad (33)$$

can be derived directly from (26)–(30).

In a *third step*, the sublattice densities ρ_ν for each single point of the curves in Fig. 5 can be superposed according to (25). In the case of the curves of Fig. 5(b), this delivers the two filled-circle curves with $\rho_1 \neq \rho_2 \neq \rho_3$ in Fig. 6. The longer curve is valid for greater positive values of $\beta v \bar{v}(13)$, while the shorter curve ending at the cross is valid for greater negative values of $\beta v \bar{v}(13)$.

For a curve of Fig. 5(a) with a medium negative value of $\beta v \bar{v}(12)$, the superposition delivers the unfilled-circle curve with $\rho_1 \equiv \rho_3 \neq \rho_2$ in Fig. 6.

The function (33) corresponding to the solution $\rho_1 \equiv \rho_2 \equiv \rho_3$ is drawn in Fig. 6 as a solid-line curve valid for greater positive values of $\beta v \bar{v}(12)$. At some greater values of $\beta v \bar{v}(12)$, the unfilled-circle curve is compressed and lies within the loop of the filled-circle curve valid for $\beta v \bar{v}(13) > 1$. In addition to these curves in Fig. 6, the function (31) is plotted for two values of $v[1-\bar{v}(12)]$ and a positive medium value of the parameter μ. The dashed curve is valid when $v[1-\bar{v}(12)] > 0$, while the alternately dashed and dotted curve is valid when $v[1-\bar{v}(12)] < 0$.

Given fixed values of βv, $\bar{v}(12)$, and $\bar{v}(13)$, the curves which represent (31) intersect the filled-circle, the unfilled-circle, and the solid-line $\rho(\lambda)$ curves in Fig. 6 at well-defined intersection

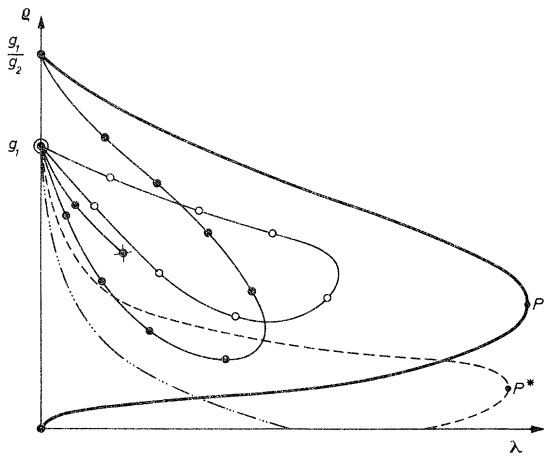

FIG. 6. Complete construction figure for the graphical determination of the $\rho(\mu)$ isotherms.

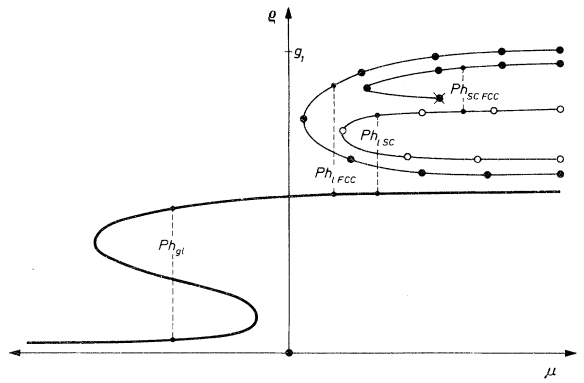

FIG. 7. $\rho(\mu)$ isotherms of the lattice model for a predominantly attractive soft particle interaction ($v > 0$) and small positive values of $\bar{v}(13)$ and $|\bar{v}(12)|$ at medium gas-liquid subcritical temperatures.

points for suitable values of the parameter μ.

In a *fourth and last step*, one can plot all the ρ coordinates of the intersection points as functions of the chemical potential μ. Such curves are drawn in Fig. 7. They are valid for medium temperatures, $v > 0$ and $0 < \bar{v}(13), \bar{v}(12) < 1$ [$|\bar{v}(12)|$ not too great] if suitable values for $\gamma, \delta, \epsilon, \varphi, \psi, \chi$ are chosen. Lines of the same type in Fig. 6 and Fig. 7 represent thereby the same density structures. The solid-line curve in Fig. 7 belongs to the structure $\rho_1 \equiv \rho_2 \equiv \rho_3$ and represents the fluid-state isotherm. The filled-circle curves belong to the structures $\rho_1 > \rho_2 > \rho_3$ and $\rho_2 > \rho_1 > \rho_3$ ($\rho_1 > \rho_3 > \rho_2$) and their higher-density branches represent the close-packed periodical density distribution with $\rho_1 > \rho_2 > \rho_3$ of the solid phase. (The combinatorial parameters $\gamma, \delta, \epsilon, \varphi, \psi, \chi$ will be chosen in the way that $\rho_1 > \rho_2 > \rho_3$ and not $\rho_1 > \rho_3 > \rho_2$ will occur.) Their lower-density branches represent the unstable structure $\rho_2 > \rho_1 > \rho_3$. The curve where the vertex lies more to the left is valid for greater positive values of $\bar{v}(13)$ than the other curve ending with a cross.

The unfilled-circle curve corresponds to the structures $\rho_1 \equiv \rho_3 > \rho_2$ and $\rho_2 > \rho_1 \equiv \rho_3$. While the higher-density branch of the isotherm represents the density distribution of the modification ($\rho_1 \equiv \rho_3 > \rho_2$), the lower-density branch represents the unstable structure $\rho_2 > \rho_1 \equiv \rho_3$. The sublattice density isotherms $\rho_\nu(\mu)$ ($\nu = 1, 2, 3$) can, of course, be drawn in the same way.

The graphical solutions of the state equations have shown that solutions like the structures $\rho_1 > \rho_3 \equiv \rho_2$ and $\rho_2 \equiv \rho_1 > \rho_3$ are not at all possible.

Concerning the influence of the interaction structure parameters $\bar{v}(12), \bar{v}(13)$ and the total negative interaction energy per lattice site v on the course of the $\rho(\mu)$ isotherms, the following statements can be given.

(1) If v becomes negative, the loops in the continuous curve of Fig. 7 are annihilated. This is also the case if the temperature increases above the gas-liquid critical point. Our model then exhibits only one fluid phase (gas), the liquid phase being prohibited.

(2) If $v\bar{v}(12)$ assumes increasing positive values, the filled- and unfilled-circle isotherms in Fig. 7 shift more and more to the left side. On the other hand, a shift of both curves to the right side in Fig. 7 is enforced if $v\bar{v}(12)$ becomes more and more negative.

(3) In a similar way, the situation of the $\rho(\mu)$ isotherms is influenced by $v\bar{v}(13)$. Positive increasing of $v\bar{v}(13)$ shifts the filled-circle curve to the left side of the unfilled-circle curve, while an increasing of $v\bar{v}(13)$ in the direction of negative values enforces a shift to the right side.

In connection with the construction of the $\rho(\mu)$ isotherms, it was stated that such reasonable isotherms as those of Fig. 7 are only valid if suitable values of the parameters $\gamma, \delta, \epsilon, \varphi, \psi, \chi$ are chosen.

What restrictions must be imposed on these parameters so that $\rho(\mu)$ isotherms like those of Fig. 7 can be calculated? The $\gamma, \delta, \epsilon, \varphi, \psi, \chi$ extensively influence the courses of the $\rho(\mu)$ isotherms at low and high densities, because they determine the courses of the $\rho(\lambda)$ curves in Fig. 6 at $\lambda \to 0$. The dependence of the $\rho(\lambda)$ curves on these parameters at $\lambda \to 0$ may therefore be discussed systematically.

First, it is clear on account of (18) and (19) that

$$\psi > 0, \quad \chi > 0 \tag{34}$$

because $\alpha(0,8)$ is positive, as are all the α's.

Second, there must be

$$\delta > 0 \tag{35}$$

because the functions (28) and therefore the corresponding function $\lambda(\rho_2)$ would otherwise exhibit an unreasonable course at $\lambda \to 0, \rho_2 \to 0$. The same can be stated concerning (33) when $\lambda \to 0, \rho \to 0$. Condition (35) ensures a reasonable low-density course of the fluid-state isotherm and is a necessary condition for a correct course of the $\rho_2(\mu)$ isotherms of the structures $\rho_1 > \rho_2 > \rho_3$ and $\rho_1 \equiv \rho_3 > \rho_2$ at high densities.

Third, a real solution of (26)–(30) with $\rho_1 \to 1$, $\rho_2 \to 0$, $\rho_3 \to 0$, $\lambda^* \to 0$, $\lambda^{**} \to 0$, $\lambda \to 0$ which exhibits the density distribution of the real close-packed structure $\rho_1 > \rho_2 > \rho_3$ must exist. (The structure $\rho_1 > \rho_3 > \rho_2$ is also of fcc symmetry, but does not represent the real density structure of close-packed hard spheres in contrast to $\rho_1 > \rho_2 > \rho_3$.) The realistic behavior of the real fcc close-packed periodical density distribution in the high-density region characterized above can certainly be expected if, in addition to (34) and (35), the following conditions are fulfilled:

$$f_1 = \delta + (g_1/g_2) f_2 + f_4 < 0, \tag{36}$$

$$-f_4 = \gamma + \epsilon + \varphi + \psi = 8z - \delta - \chi,$$

$$f_2 = \epsilon + 2\varphi + 3\psi + 2\chi > 0. \tag{37}$$

If (36) and (37) are valid, a regular high-density solution of the structure $\rho_1 > \rho_2 > \rho_3$, represented by the higher-density branches of the filled-circle curves in Fig. 7, can always be constructed with

$$1 - \rho_1 \sim (\exp\{\beta v[\bar{v}(13) + \bar{v}(12)]/2\}\lambda)^{1/(8z-\delta)}, \tag{38}$$

$$\rho_2 \sim (\exp\{-\beta v[\bar{v}(13) + \bar{v}(12)]/2\})^{[\chi + (g_1/g_2)f_2]/(8z-\delta)\delta} \lambda^{-[f_4 + (g_1/g_2)f_2]/(8z-\delta)\delta}, \tag{39}$$

$$\rho_3 \sim [\exp[-\beta v \bar{v}(13)](\exp\{\beta v[\bar{v}(12) + \bar{v}(13)]/2\})^{-f_4/(8z-\delta)}]^{1/\delta} \lambda^{-f_4/(8z-\delta)\delta}, \tag{40}$$

$$g_1 - \rho \sim 1 - \rho_1, \tag{41}$$

$$(1 - \rho/g_1)^{8z} \exp(\beta\{v[1 - \bar{v}(12)]\rho + \mu\}) \sim \lambda, \tag{42}$$

whereby (20) is used.

If the condition (36) is violated, (26), (29), and (30) can become complex functions which should be excluded. Condition (37) ensures the structure $\rho_1 > \rho_2 > \rho_3$. The lower-density branches of the filled-circle curves in Fig. 7 are then also represented correctly.

Fourth, a real solution of (26)–(30) with $\rho_1 \equiv \rho_3 \to \frac{1}{2}, \rho_2 \to 0, \lambda^* \to 0, \lambda^{**} \to 0, \lambda \to 0$ which exhibits a reasonable high-density behavior of the structure $\rho_1 \equiv \rho_3 > \rho_2$ (modification) must exist. The corresponding condition which must be demanded is

$$f_3 = \delta - 2(g_1/g_2)\chi < 0. \tag{43}$$

Otherwise, the functions (29) and (30) can become complex. If (43) is fulfilled, a regular high-density solution of the structure $\rho_1 \equiv \rho_3 > \rho_2$ representing the higher-density branch of the unfilled-circle curve in Fig. 7, can always be constructed with

$$1 - (\rho_1 + \rho_3) \sim \{2^{8z-\chi} \exp[\beta v \bar{v}(12)/2]\lambda\}^{1/\chi}, \tag{44}$$

$$\rho_2 \sim (2^A \exp\{(2g_1/g_2 - 1)\beta v[\bar{v}(13) + \bar{v}(12)]/2\} \lambda^{2g_1/g_2})^{1/\delta}, \tag{45}$$

where $A = (2g_1/g_2 - 1)(8z - \chi) + 2(g_1/g_2)(f_2 - 2\chi)$,

$$g_1 - \rho \sim 1 - (\rho_1 + \rho_3), \tag{46}$$

and (42). A regular high-density solution of the structure $\rho_2 > \rho_1 \equiv \rho_3$ which represents the lower-density branch of the unfilled-circle curve in Fig. 7 then also exists, whereby

$$\rho_1 + \rho_3 \sim 2 \times 3^{\chi/\delta} \lambda^{1/\delta}, \tag{47}$$

$$1 - \frac{g_2}{g_1}\rho_2 \sim \left\{ \left(\frac{g_2}{g_2 - g_1}\right)^{\gamma} \left(\frac{g_2}{g_1}\right)^{\delta} \left[\left(\frac{g_2}{g_2 - 2g_1}\right)^{4\epsilon} \left(\frac{g_2}{g_2 - 3g_1}\right)^{2\varphi} \right]^{g_1/g_2} \exp\left(\frac{\beta v \bar{v}(12) g_1}{g_2}\right) \right.$$
$$\left. \times \left[\left(\frac{g_2}{g_2 - g_1}\right)^{\epsilon} \left(\frac{g_2}{g_2 - 2g_1}\right)^{2\varphi} \left(\frac{g_2}{g_2 - 3g_1}\right)^{3\psi} \right]^{2g_1/g_2} \left(\frac{g_2}{g_2 - 4g_1}\right)^{-\chi(2g_1/g_2 - 1)} \lambda \right\}^{(g_2/2g_1)/\chi}, \tag{48}$$

$$g_1 - \rho \sim 1 - (g_2/g_1)\rho_2, \tag{49}$$

and (42) are valid.

Fifth, for arbitrary values of βv, $\bar{v}(12)$, and $\bar{v}(13)$, we expect that, at high densities, the densities of the higher-density branches of the filled-circle curves in Fig. 7 (fcc close-packed structure $\rho_1 > \rho_2 > \rho_3$) are greater than the density of the higher-density branch of the unfilled-circle curve in Fig. 7 (sc structure $\rho_1 \equiv \rho_3 > \rho_2$), because it seems physically reasonable that the substance is more compressed in the fcc close-packed structure than in the sc structure or the liquid structure. This demands that the slopes of the filled-circle $\rho(\lambda)$ curves in Fig. 6 must be more negative than the slope of the unfilled-circle $\rho(\lambda)$ curve at $\lambda \to 0$. The condition

$$f_4 = \delta - (8z - \chi) < 0 \tag{50}$$

ensures, on account of (38), (41), (44), and (46), that the filled- and unfilled-circle $\rho(\mu)$ isotherms in Fig. 7 exhibit the behavior demanded above at higher densities.

IV. DETERMINATION OF THE STABLE PHASES AND THEIR DOMAINS OF STABILITY

In the preceding section, we determined all the solutions of the state equations (21)–(25) in the whole μ domain. It now remains to be shown which branches of the solutions represent stable phases and in which ranges of the μ domain the single phases are defined.

The questions posed above can be answered by a plotting of the $p(\mu)$ isotherms corresponding to the $\rho(\mu)$ isotherms of Fig. 7. The $p(\mu)$ isotherms can be calculated with the aid of (6) and (13), or simply by (24) if at least one point of an isotherm is known.

In Fig. 8, $p(\mu)$ isotherms directly derived from the $\rho(\mu)$ isotherms of Fig. 7 are plotted. Correspondingly drawn curves in Fig. 7 and Fig. 8 have the same meaning; that is, they represent the same density structures. The $p(\mu)$ isotherms in Fig. 8 are valid for the same values of v, $\bar{v}(13)$, $\bar{v}(12)$, and $\delta, \gamma, \epsilon, \varphi, \psi, \chi$ as the $\rho(\mu)$ isotherms in Fig. 7.

As in Fig. 7, one recognizes in Fig. 8 that there are a greater number of branches of the $\rho(\mu)$ or $p(\mu)$ functions in certain ranges of the μ domain. There is, however, only one branch in a given bounded range of the μ domain which is of physical interest and which can be selected uniquely. This is the branch characterized by a maximum pressure. In the corresponding μ range it represents a thermodynamically stable phase. Two possibilities are considered in Fig. 8.

In the first case $[0 < \bar{v}(13), \bar{v}(12) < 1, |\bar{v}(12)|$ not too great, $\bar{v}(13)$ not too small$]$, we find three stable phases: a gas phase represented in the interval $-\infty \leq \mu \leq \mu(Ph_{g\,1})$ by the solid-line low-density branch of the structure $\rho_1 \equiv \rho_2 \equiv \rho_3$, a liquid phase represented in the interval $\mu(Ph_{g\,1}) \leq \mu \leq \mu(Ph_{l\,\mathrm{fcc}})$ by the solid-line high-density branch of the structure $\rho_1 \equiv \rho_2 \equiv \rho_3$, and a solid phase represented in the interval $\mu(Ph_{l\,\mathrm{fcc}}) \leq \mu \leq \infty$ by the filled-circle higher-density branch which belongs to the structure $\rho_1 > \rho_2 > \rho_3$. We would expect isotherms like that

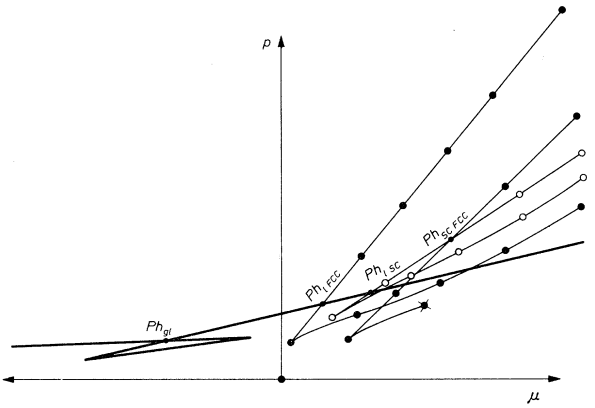

FIG. 8. $p(\mu)$ isotherms of the lattice model for a predominantly attractive soft particle interaction ($v > 0$) and small positive values of $\bar{v}(13)$ and $|\bar{v}(12)|$ at medium gas-liquid subcritical temperatures.

of the first case for inert gases.

In the second case [$\bar{v}(13) \lesssim 0, \bar{v}(12) < 1, |\bar{v}(12)|$ not too great], again in the intervals $-\infty \leq \mu \leq \mu(Ph_{g\,1})$ and $\mu(Ph_{g\,1}) \leq \mu \leq \mu(Ph_{1\,sc})$, a gas and a liquid phase, represented by the solid-line isotherms, are found to be stable. But now a new phase, the modification, occurs. This is stable in the range $\mu(Ph_{1\,sc}) \leq \mu \leq \mu(Ph_{sc\,fcc})$ and is represented by the unfilled-circle higher-density branch which belongs to the structure $\rho_1 \equiv \rho_3 > \rho_2$. At high pressures in the interval $\mu(Ph_{sc\,fcc}) \leq \mu \leq \infty$, again the structure $\rho_1 > \rho_2 > \rho_3$ represented by the higher-density branch of the filled-circle curve, delivers a stable phase. The isotherm of the second case describes the pressure behavior of a four-phase system, as, for example, sulfur.

The edges of the ranges of stability determine phase-transition points $Ph_{g\,1}, Ph_{1\,fcc}, Ph_{1\,sc}, Ph_{sc\,fcc}$ where the stable branches cross over. The densities jump unsteadily at these points and form curves of coexistence if plotted as functions of the temperature. The transition densities are linked in Fig. 7 by thin dotted lines.

$Ph_{g\,1}$ indicates a gas-liquid transition, $Ph_{1\,fcc}$ a liquid-solid transition, $Ph_{1\,sc}$ a liquid-modification transition and $Ph_{sc\,fcc}$ a modification-solid transition. *All transitions are of first order for all temperatures.*

Concerning the dependence of the $p(\mu)$ isotherms on the interaction structure parameters $\bar{v}(12)$ and $\bar{v}(13)$ and on the total negative interaction energy per lattice site v, analogous statements can be given as for the $\rho(\mu)$ isotherms in the paragraphs (1)–(3) of Sec. III.

Apart from the isotherms drawn in Fig. 8, still other $p(\mu)$ isotherms describing essentially different thermodynamical systems exist. These are a three-phase system (gas-modification-solid with a gas-modification transition and a modification-solid transition) and a two-phase system (gas-solid with a gas-solid transition). For the values of v, $\bar{v}(12)$, and $\bar{v}(13)$ used in Fig. 7 and Fig. 8, the three-phase system is, for example, stable at higher temperatures and the two-phase system is stable at lower temperatures. Negative values of v enlarge the temperature domain of stability for both systems. Increasing of $\bar{v}(12)$ extends the temperature domain of stability of the three-phase system, while increasing of $\bar{v}(13)$ extends the temperature domain of stability for the two-phase system.

Concerning the influence of the combinatorial parameters on the $p(\mu)$ isotherms, one can state that the restrictive conditions (34), (35), (36), (37), (43), and (50) postulated in respect of a reasonable course of the $\rho(\mu)$ isotherms are necessary but not sufficient conditions for a reasonable course of the $p(\mu)$ isotherms. Further restrictive conditions must therefore be found. They can be obtained by a discussion of the behavior of the high respectively low-pressure asymptotes of the $p(\mu)$ isotherms. With the aid of (6) and (13), the asymptotic behavior of all branches of the $p(\mu)$ isotherms can be easily investigated.

For the low-pressure limit of the gas phase,

$$p_g \to 0, \quad \rho_g \to 0, \quad \mu \to -\infty \tag{51}$$

is valid, while for the high-pressure limit of the liquid phase,

$$\begin{aligned} &p_l \to g_1[\tfrac{1}{2}(g_1 v + 2\mu) + (1/\beta) f_5], \\ &\rho_l \to g_1, \quad \mu \to +\infty \end{aligned} \tag{52}$$

with

$$\begin{aligned} f_5 = {} & \delta \ln 8 + 7\gamma \ln(\tfrac{7}{8}) + 3\epsilon \ln(\tfrac{6}{8}) \\ & + \tfrac{5}{3}\varphi \ln(\tfrac{5}{8}) + \psi \ln(\tfrac{4}{8}) + \tfrac{1}{3}\chi \ln(\tfrac{2}{8}) \end{aligned} \tag{53}$$

can be proved.

At high pressures for the modification [consider the higher-pressure branch of the unfilled-circle $p(\mu)$ isotherm in Fig. 8], the following limits are found:

$$\begin{aligned} &p_{sc} \to g_1(\tfrac{1}{2}\{g_1 v[1 + 3\bar{v}(12)] + 2\mu\} + (1/\beta) f_6), \\ &\rho_1^{(sc)} \to \tfrac{1}{2}, \quad \rho_3^{(sc)} \to \tfrac{1}{2}, \quad \rho_2^{(sc)} \to 0, \quad \mu \to \infty, \end{aligned} \tag{54}$$

with

$$f_6 = 2\delta - (8z - \chi) = \delta + f_4. \tag{55}$$

The solid phase [consider the higher-pressure branches of the filled-circle $p(\mu)$ isotherms in Fig. 8] is characterized by the following high-pressure limits:

$$\begin{aligned} &p_{fcc} \to \tfrac{1}{2} g_1 \{g_1 v[1 + 3\bar{v}(12) + 4\bar{v}(13)] + 2\mu\}, \\ &\rho_1^{(fcc)} \to 1, \quad \rho_2^{(fcc)} \to 0, \quad \rho_3^{(fcc)} \to 0, \quad \mu \to +\infty. \end{aligned} \tag{56}$$

The high-pressure limits of the structures $\rho_2 > \rho_1 > \rho_3$ and $\rho_2 > \rho_1 \equiv \rho_3$ which belong to the lower-density branches of the filled- and unfilled-circle $p(\mu)$ isotherms in Fig. 8 can be calculated only approximately because the limits of the sublattice densities ρ_ν are not known exactly in every case. On account of (24) and the course of the corresponding $\rho(\mu)$ isotherms in Fig. 7, their high-pressure limits must however be lower than those of the structure $\rho_1 > \rho_2 > \rho_3$ (56) and the structure $\rho_1 \equiv \rho_3 > \rho_2$ (54).

For the high-density behavior of the $\rho(\mu)$ isotherms in Fig. 7, it was discussed that

$$\rho_{fcc} > \rho_{sc} > \rho_1 \tag{57}$$

is physically reasonable for arbitrary values of βv, $\bar{v}(12)$, and $\bar{v}(13)$. Consistently, it may be demanded that, at high pressures,

$$p_{\mathrm{fcc}} > p_{\mathrm{sc}} > p_1 \tag{58}$$

is valid in a large region of temperature,

$$0 < \beta < \beta_{\mathrm{lim}} \tag{59}$$

whereby β_{lim} depends on v, $\bar{v}(12)$, and $\bar{v}(13)$. In connection with (57), the condition (58) also appears physically reasonable because the pressure in a structure of greater density should be greater. The condition (58) delivers a further restriction of the combinatorial parameters $\gamma, \delta, \epsilon, \varphi, \psi, \chi$. On account of (52)–(56),

$$f_5 < f_6 < 0. \tag{60}$$

The relation (58) is violated at temperatures where the asymptotes (52), (54), and (56) begin to cross at infinitely high pressures.

The temperature where p_1 and p_{fcc} of (52) and (56) cross is defined by

$$\beta_{1\,\mathrm{fcc}}\, v[3\bar{v}(12) + 4\bar{v}(13)] = (2/g_1) f_5. \tag{61}$$

The temperature where p_1 and p_{sc} of (52) and (54) cross is defined by

$$\beta_{1\,\mathrm{sc}}\, v\bar{v}(12) = (2/3g_1)(f_5 - f_6). \tag{62}$$

A crossing over of p_{fcc} and p_{sc} finally occurs at the temperature defined by

$$\beta_{\mathrm{sc\,fcc}}\, v\bar{v}(13) = (1/2g_1) f_6. \tag{63}$$

At the temperatures defined by (61)–(63), the corresponding pressure-temperature phase-transition curves have high-pressure asymptotes (compare Figs. 10). The lower bound β_{lim} of the interval (59) is given by the maximum of $\beta_{1\,\mathrm{fcc}}, \beta_{1\,\mathrm{sc}}, \beta_{\mathrm{sc\,fcc}}$ defined in (61)–(63). With the aid of (52)–(63), one recognizes that when $v\bar{v}(12) > 0$ and $v\bar{v}(13) > 0$ the relation (58) is valid for all temperatures; otherwise, only in the finite interval (59).

The restrictive conditions (34)–(37), (43), (50), (53), (55) confine the possible values of the combinatorial parameters severely but they do not fix them uniquely. This may be illustrated in Fig. 9. On account of (18)–(20), (34), and (35), the possible values of $\gamma, \delta, \epsilon, \varphi, \psi, \chi$ can be represented as points in the upper half ($\delta > 0$) of the three-dimensional $\delta, \epsilon, \varphi$ space. The relations

$$\begin{aligned} &f_1 \equiv 0, \quad f_2 \equiv 0, \quad f_3 \equiv 0, \\ &f_4 \equiv 0, \quad f_5 \equiv 0, \quad f_6 \equiv 0, \end{aligned} \tag{64}$$

whereby the f_ν are the functions defined in (36), (37), (43), (50), (53), (55), represent a group of planes in the $\delta, \epsilon, \varphi$ space with group parameter χ on account of (18)–(20). The planes $f_3 \equiv 0$, $f_4 \equiv 0$, $f_6 \equiv 0$ are parallel to the plane $\delta \equiv 0$, while the plane $f_2 \equiv 0$ is vertical to the plane $\delta \equiv 0$. The condition (50) is automatically valid if the condition (60) is fulfilled. The group parameter χ is bounded on account of (34), (35), (55), (60) to the region

$$0 \leq \chi \leq 8z. \tag{65}$$

On the other hand, the discussion of the high-pressure behavior of the $p(\mu)$ isotherms by means of (52)–(56) shows that $p(\mu)$ isotherms which describe more than two phases can, in principle, only occur if

$$|f_5| \ll 1, \quad |f_6| \ll 1. \tag{66}$$

The condition (66) in connection with (43) and (55) entails that the plane $f_3 \equiv 0$ must lie above the plane $f_6 \equiv 0$ or both planes must at least coincide. Therefore the condition

$$\chi \geq \tfrac{24}{5} z \tag{67}$$

must be fulfilled.

In Fig. 9, the plane $f_3 \equiv f_6 \equiv 0$ with $\chi = \frac{24}{5} z$ is chosen as a coordinate plane for the coordinates ϵ, φ. The straight lines f_1-f_6, f_2-f_6, and f_5-f_6 represent the intersection lines of the planes $f_1 \equiv 0$, $f_2 \equiv 0$, and $f_5 \equiv 0$ with the plane $f_6 \equiv 0$ or $f_3 \equiv 0$. The signs + and – indicate that the functions f_1, f_2, f_5 are positive or negative in the corresponding half-planes. A small hatched zone between the intersection points S and R in Fig. 9 lying just below the plane $f_6 \equiv f_3 \equiv 0$ designates the values of $\gamma, \delta, \epsilon, \varphi, \psi, \chi$, where the conditions (34)–(37), (43), (50), (60), (65) and especially (66) and (67) are all simultaneously fulfilled. Test calculations performed for points of the hatched zone show that points lying in the close neighborhood of the intersection point S deliver most reasonable $\rho(\mu)$ and $p(\mu)$ isotherms and phase diagrams as drawn in Fig. 10.

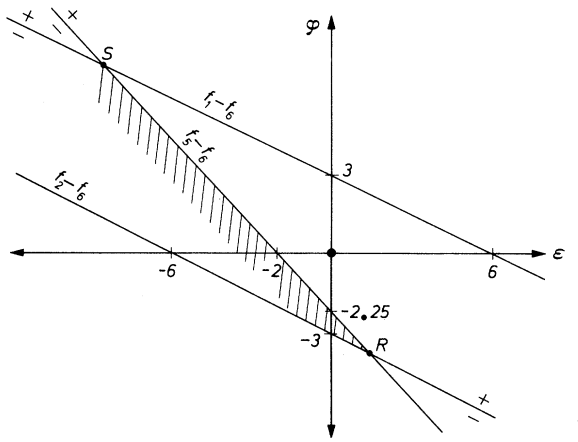

FIG. 9. Illustration of the $\delta, \epsilon, \varphi$ subspace consisting of all those points which correspond to compatible values of the combinatorial parameters $\delta, \chi, \epsilon, \varphi$. The scale is chosen in units of χ.

V. EQUATION OF STATE OF THE FLUID PHASES

For the calculation of the fluid-phase isotherms, the cumbersome graphical construction need not be used as a comparatively simple analytical expression can be derived directly from the general state equations (6), (13), (21)–(25) by the assumption $\rho_1 \equiv \rho_2 \equiv \rho_3 \equiv \rho$. The result is the following state equation:

$$p = -\tfrac{1}{2} v \rho^2 + \frac{1}{\beta} \ln\left(\frac{(1-\rho)^{\gamma}(1-2\rho)^{\epsilon/2}(1-3\rho)^{\varphi/3}(1-4\rho)^{\psi/4}(1-6\rho)^{\chi/6}}{(1-\rho/g_1)^{z}} \right). \tag{68}$$

The critical density ρ_{cgl} and the critical temperature $T_{cgl} = 1/k\beta_{cgl}$ of the gas-liquid transition can be easily determined from (68) by $d^2p/d\rho^2 = 0$ and $dp/d\rho = 0$ respectively; that is, by

$$\frac{\gamma}{(1-\rho_{cgl})^2} - \frac{\delta}{(\rho_{cgl})^2} + \frac{4\epsilon}{(1-2\rho_{cgl})^2} + \frac{9\varphi}{(1-3\rho_{cgl})^2} + \frac{16\psi}{(1-4\rho_{cgl})^2} + \frac{36\chi}{(1-6\rho_{cgl})^2} - \frac{z/g_1^3}{(1-\rho_{cgl}/g_1)^2} = 0 \tag{69}$$

and

$$\beta_{cgl} v = \frac{\delta}{\rho_{cgl}} - \frac{\gamma}{1-\rho_{cgl}} - \frac{2\epsilon}{1-2\rho_{cgl}} - \frac{3\varphi}{1-3\rho_{cgl}} - \frac{4\psi}{1-4\rho_{cgl}} - \frac{6\chi}{1-6\rho_{cgl}} + \frac{z/g_1^2}{1-\rho_{cgl}/g_1}. \tag{70}$$

The values of β_{cgl} and ρ_{cgl} can be inserted in (6), (13), and (21)–(23), delivering the critical chemical potential μ_{cgl} and the critical pressure p_{cgl}. Equation (69) has for values of $\gamma, \epsilon, \delta, \varphi, \psi, \chi$ determined in the way which was discussed at the end of Sec. IV (ϵ, φ lying at the point S in Fig. 9) only one root ρ_{cgl} in the interval $0 \leq \rho \leq g_1$. The critical data are then

$$\rho_{cgl} = 0.06, \quad \beta_{cgl} v = 63.20,$$

$$\mu_{cgl} = -0.11v, \quad p_{cgl} = 0.011v.$$

VI. RESULTS AND DISCUSSION

Among the most important results which can be obtained for our model are the phase-transition curves of a pressure-temperature phase diagram. In Fig. 10, the phase-transition curves of our model (corresponding to the transition points $Ph_{g\,1}$, $Ph_{1\,fcc}, Ph_{1\,sc}, Ph_{sc\,fcc}$ in Fig. 8) are drawn in a p-βv diagram for fixed characteristic values of a predominantly attractive soft interaction ($v > 0$) and the interaction structure parameters $\bar{v}(12)$ and $\bar{v}(13)$. *They all represent transitions of the first order.* The fluid-solid and the solid-solid transition curves extend up to infinitely high pressures and temperatures.

Figure 10(a) represents a typical and realistic phase diagram for the three-phase system (gas-liquid-solid) of inert gases. It is valid when $v > 0, \bar{v}(12) < 0, \bar{v}(13) > 0, 3\bar{v}(12) + 4\bar{v}(13) > 0, |3\bar{v}(12) + 4\bar{v}(13)| \ll 1, |\bar{v}(12)| \gg 1$. Figures 10(b) and 10(c) represent four-phase diagrams of our model. They are valid when $v > 0, \bar{v}(12) > 0, \bar{v}(13) > 0, |\bar{v}(12)| \ll 1, |\bar{v}(13)| \ll 1$. For Fig. 10(c), $|\bar{v}(13)|$ is in addition comparatively smaller than for Fig. 10(b). Figures 10(e)–10(g) also represent four-phase diagrams. They are valid when $v > 0, \bar{v}(12) < 0, \bar{v}(13) > 0, 3\bar{v}(12) + 4\bar{v}(13) < 0, |\bar{v}(13)| \ll 1$; $v > 0, \bar{v}(12) > 0, \bar{v}(13) < 0, 3\bar{v}(12) + 4\bar{v}(13) \lesssim 0, |\bar{v}(12)| \ll 1$; $v > 0, \bar{v}(12) < 0, \bar{v}(13) < 0, |\bar{v}(12)| \ll 1, |\bar{v}(13)| \gg 1$, respectively. Some fluid-solid and solid-solid transition curves of these diagrams exhibit rather peculiar courses at lower temperatures. They have high-pressure asymptotes at temperatures defined by (61)–(63). The same can be stated concerning the liquid-solid transition curve of a gas-liquid-solid system drawn in Fig. 10(d) which is valid when $v > 0, \bar{v}(12) < 0, \bar{v}(13) > 0, 3\bar{v}(12) + 4\bar{v}(13) < 0, |\bar{v}(12)| \gg 1, |\bar{v}(13)| \gg 1$. In Figs. 10(h) and 10(i), the transition curves of other three-phase systems without any liquid phase are drawn. They are valid when $v > 0, \bar{v}(12) > 0, \bar{v}(13) > 0, |\bar{v}(12)| \gg 1, |\bar{v}(13)| \ll 1$ and $v > 0, \bar{v}(12) > 0, \bar{v}(13) < 0, 3\bar{v}(12) + 4\bar{v}(13) \lesssim 0, |\bar{v}(12)| \gg 1$, respectively. The sc-fcc transition curve in Fig. 10(i) again has an asymptote defined by (63). In Fig. 10(j), a phase diagram of a gas-solid system is presented; this is valid when $v > 0, \bar{v}(12) < 0, \bar{v}(13) > 0, 3\bar{v}(12) + 4\bar{v}(13) \gg 1, |\bar{v}(12)| \gg 1$.

In the case of a predominantly repulsive interaction ($v < 0$), qualitatively the same phase diagrams will occur but without any gas-liquid transition curves. The gas-liquid transition curves are determined by v only, while the other transition curves are determined by $v\bar{v}(12)$ and $v\bar{v}(13)$. $\bar{v}(12)$ and $\bar{v}(13)$ are then group parameters which designate for fixed v a group of transition curves and therefore a group of phase diagrams.[44,45] In Fig. 10, only a few characteristic diagrams are selected. Numerous intermediate diagrams in which the triple points T_2 and T_1 are shifted are possible.

Transition curves as drawn in Fig. 10 will only result if the parameters $\gamma, \delta, \epsilon, \varphi, \psi, \chi$ are chosen in the way discussed at the end of Sec. IV (most adapted MQC approximation).[44,45] If $\gamma, \delta, \epsilon, \varphi,$

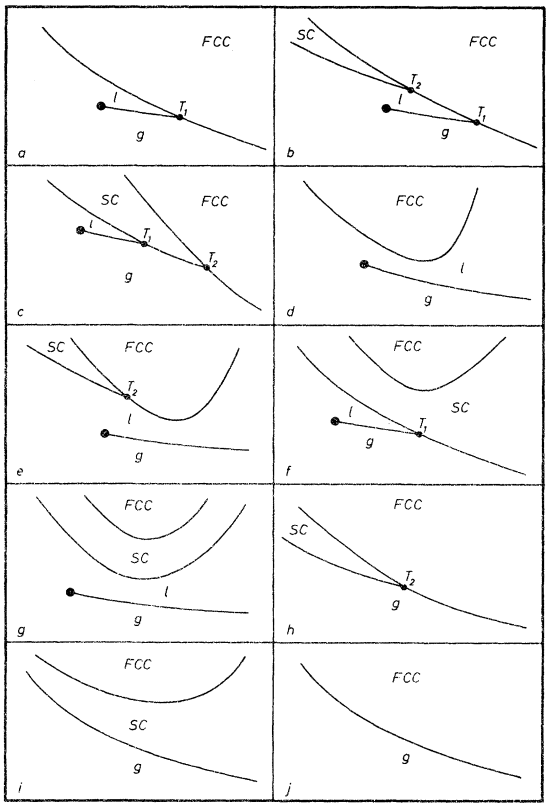

FIG. 10. Most important different types of the p-βv phase diagrams of the lattice model for a predominantly attractive soft particle interaction ($v > 0$). The pressure p is taken as the ordinate, while $\beta v = v/kT$ is taken as the abscissa. The various areas where stable phases exist are designated by the abbreviations: g = gas phase, l = liquid phase, sc = simple-cubic modification phase, fcc = solid phase with face-centered-cubic structure. The filled circles at the ends of the gas-liquid transition curves designate the gas-liquid critical points. The points T_1 designate gas-liquid-solid triple points while the points T_2 designate fluid-solid-solid triple points.

ψ, χ are chosen without considering (66), diagrams like Fig. 10(a) and Figs. 10(b) and 10(c) cannot occur. Instead of these diagrams, only diagrams like Figs. 10(h), 10(i) and Fig. 10(j) without any liquid phase will result. This is also true if one uses the QC approximation $\alpha(0, l_1, -, l_m, l_n) \equiv 1$ which corresponds to the point

$$\delta = 1 + 2z(2z - 7),$$

$$\gamma = -1 + 49z/6, \quad \epsilon = -z(1 + 3z),$$

$$\varphi = z(2 - z), \quad \psi = 22z/3, \quad \chi = 11z/2,$$

in the $\delta, \epsilon, \varphi, \chi$ space which is not within the hatched zone of Fig. 9. It is again confirmed that QC approximations of the combinatorial factor W_{hc}, although very successful in the case of conventional Ising lattice models,[35-37] do not seem to deliver as good phase diagrams for hard-core lattice models as optimal adapted MQC approximations.[44,45] If the functions f_5 and f_6 from (53) and (55) become positive, one obtains MQC transition curves for the fluid-solid and solid-solid transitions only when $v\bar{v}(12) > 0, v\bar{v}(13) > 0$. These transition curves, however, exhibit an unreasonable behavior at high pressures and temperatures, like corresponding curves of other models drawn in Fig. 11 of Ref. 45. The dependence of the phase diagrams on the combinatorial parameters therefore seems to be very similar for all the investigated models.[44,45]

The phase diagrams in Fig. 10 now clearly exhibit the connection between the thermodynamic behavior of our model and the geometrical structure of the interaction. One recognizes that increasing of $v\bar{v}(12)$ in the positive direction generally favors crystalline structures against liquid structures, even at lower pressures and temperatures, while an increase in the negative direction leads to multiphase systems, where the crystalline structures occur only at higher pressures and temperatures. The occurrence of a close-packed fcc structure at lower pressures and temperatures is favored against the existence of sc or liquid structures at large positive values of $v\bar{v}(13)$, while in the case of large negative values of $v\bar{v}(13)$, close-packed fcc structures are also generated, but at higher pressures and temperatures. The macroscopic thermodynamic response of our model on the microscopic influence by the particle interaction seems to be intelligible from the physical point of view.

In this way, our model describes the thermodynamical properties of inert gases well, by the phase diagram Fig. 10(a). We know from inert gases that their atoms interact by a short hard-core and a long-range, comparatively slowly-varying, predominantly attractive particle interaction which is rather independent of the temperature. This interaction is also comparatively weak; therefore liquid structures can occur. Otherwise, we would observe diagrams as Fig. 10(j).

In nature, there are some substances which occur in two fluid and two solid phases like our model. An example is sulfur. On the other hand, there is no substance known to the author which exhibits a phase diagram which is completely congruent with one of the four-phase diagrams of our model plotted for fixed values of v, $\bar{v}(12)$ and $\bar{v}(13)$ in Figs. 10(b)–10(g). It also seems to be difficult to find in nature systems consisting of a gas phase and two or one solid phases which exhibit phase diagrams like those drawn in Figs.

10(h)–10(j).

The reason is that, in the case of real substances which occur in more than one solid phase, the interaction in the substance is built up by complicated chemical bonds. The interaction is then probably temperature dependent; that is, one must assume suitable temperature functions for $\bar{v}(12)$ and $\bar{v}(13)$. Examples of such functions are plotted in Fig. 11.

If we for our model consider the temperature functions of $\bar{v}(12)$ and $\bar{v}(13)$ of Fig. 11 while v is kept fixed, a phase diagram with three triple points T_1, T_2, T_3 such as that drawn in Fig. 12 results. One need only consider the $\bar{v}(12)$ and $\bar{v}(13)$ functions of Fig. 11 in a phase diagram where the complete group of the transition curves for all values of the group parameters $\bar{v}(12)$ and $\bar{v}(13)$ is drawn.

A comparison of the diagram Fig. 12 with the phase diagrams of Fig. 10 shows that the diagram of Fig. 12 is composed of three parts: a low-temperature part in the region $\beta(T_2) \leq \beta \leq \infty$ which is similar to the diagram Fig. 10(c); a high-temperature part in the region $0 \leq \beta \leq \beta(T_3)$ which is similar to the diagram Fig. 10(a); a medium temperature part in the region $\beta(T_3) \leq \beta \leq \beta(T_2)$ which

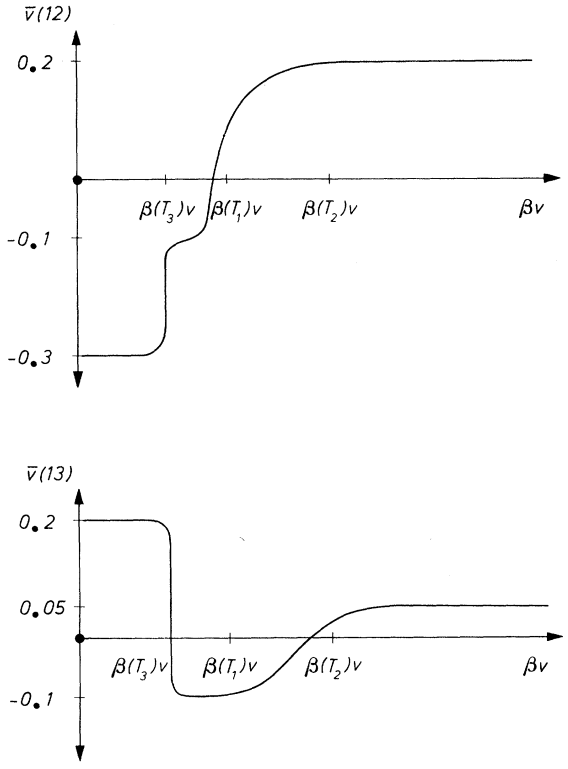

FIG. 11. A possible dependence of the interaction structure parameters $\bar{v}(12)$ and $\bar{v}(13)$ on βv which entails the sulfur-type phase diagram of Fig. 12.

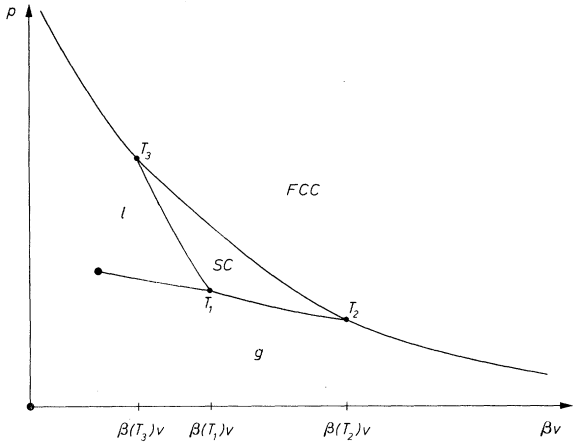

FIG. 12. A four-phase sulfur-like p-βv phase diagram with three different triple points T_1, T_2, T_3 and one heavily drawn gas-liquid critical point. This diagram is obtained for a fixed value of v and an assumed temperature dependence of $\bar{v}(12)$ and $\bar{v}(13)$ on βv as sketched in Fig. 11. The areas of stable phases are designated in the same way as in Fig. 10.

is similar to Figs. 10(g) and 10(f) in corresponding subregions of $[\beta(T_3), \beta(T_2)]$.

The phase diagram Fig. 12 is now identical with that of sulfur if one identifies the rhombic modification, the monocline modification, the liquid and the gas phase of the sulfur with the close-packed fcc structured solid phase, the sc structured modification, and the liquid and the gas phase of our model, respectively. It is perhaps also possible that at least parts of phase diagrams of other real substances occurring in nature can be represented by phase diagrams of our model if a suitable temperature dependence $\bar{v}(12)(\beta v), \bar{v}(13)(\beta v)$ is assumed.

The results obtained for our hard-core compound lattice model have shown that the phase-transition behavior of inert gases and also sulfur can be understood, in principle, on the basis of this model. The fcc close-packed density structure of the solid phase of inert gases is well reproduced thereby.

The two crystalline modifications of our model which have been identified with the corresponding solid modifications of sulfur do not exhibit density structures that are very true to nature. The inexact reproduction of density structures of phases is however a general lack of lattice models. The lack can be probably removed by increasing the number of lattice sites and sublattices, whereby the volume of the system and the radius of the hard core is kept fixed.[4-7,30] The derivation and solution of the corresponding state equations will surely then lead to very difficult mathematical

problems, whereby the insight into the connection between thermodynamical properties of the model and the interaction structure may perhaps be lost. It therefore seems reasonable to show by more simple, although more unrealistic, models that the thermodynamical behavior of real substances can be understood, in principle, by means of statistical-mechanical theories before more realistic but much more complicated models are investigated.

[1]A. Münster, *Statistical Thermodynamics* (Academic, New York, 1969), Vol. I (See also references therein).
[2]T. D. Lee and C. N. Yang, Phys. Rev. 87, 410 (1952).
[3]C. Domb and M. F. Sykes, Adv. Phys. 9, 245 (1960).
[4]B. J. Alder and T. E. Wainwright, J. Chem. Phys. 33, 1439 (1960).
[5]B. J. Alder and T. E. Wainwright, Phys. Rev. 127, 359 (1962).
[6]W. W. Wood and J. D. Jacobson, J. Chem. Phys. 27, 1207 (1957).
[7]W. W. Wood, F. R. Parker, and J. D. Jacobson, Nuovo Cimento 9, Suppl. 1, 133 (1958).
[8]C. Domb, Nuovo Cimento 9, Suppl. 1, 9 (1958).
[9]H. N. V. Temperley, Proc. Phys. Soc. A 67, 233 (1954).
[10]H. N. V. Temperley, Proc. Phys. Soc. B 70, 536 (1957).
[11]H. N. V. Temperley, Proc. Phys. Soc. (Lond.) 74, 183 (1959); 74, 432 (1959).
[12]H. N. V. Temperley, Proc. Phys. Soc. B 77, 630 (1961).
[13]H. N. V. Temperley, Proc. Phys. Soc. (Lond.) 80, 813 (1962); 80, 823 (1962).
[14]D. M. Burley, Proc. Phys. Soc. (Lond.) 75, 262 (1960).
[15]D. M. Burley, Proc. Phys. Soc. (Lond.) 77, 451 (1961).
[16]D. M. Burley, Proc. Phys. Soc. B 85, 1173 (1965).
[17]D. S. Gaunt and M. E. Fisher, J. Chem. Phys. 43, 2840 (1965).
[18]F. H. Ree and D. A. Chesnut, J. Chem. Phys. 45, 3983 (1966).
[19]L. K. Runnels and L. L. Combs, J. Chem. Phys. 45, 2482 (1966).
[20]L. K. Runnels, Phys. Rev. Lett. 15, 581 (1965).
[21]L. K. Runnels, J. Math. Phys. 8, 2081 (1967).
[22]F. H. Ree and D. A. Chestnut, Phys. Rev. Lett. 18, 5 (1967).
[23]D. S. Gaunt, J. Chem. Phys. 46, 3237 (1967).
[24]A. Bellemans and R. K. Nigam, J. Chem. Phys. 46, 2922 (1967).
[25]J. Orban and A. Bellemans, J. Chem. Phys. 49, 363 (1968).
[26]L. K. Runnels, J. Math. Phys. 11, 842 (1970).
[27]L. K. Runnels, J. P. Salvant, and H. R. Streiffer, J. Chem. Phys. 52, 2352 (1970).
[28]L. K. Runnels, J. R. Craig, and H. R. Streiffer, J. Chem. Phys. 54, 2004 (1971).
[29]J. Orban, J. V. Craen, and A. Bellemans, J. Chem. Phys. 49, 1778 (1968).
[30]W. G. Hoover, B. J. Alder, and F. H. Ree, J. Chem. Phys. 41, 3528 (1964).
[31]J. L. Lebowitz and O. Penrose, J. Math. Phys. 7, 98 (1966).
[32]D. J. Gates and O. Penrose, Commun. Math. Phys. 15, 255 (1966).
[33]G. Stell, H. Narang, and C. K. Hall, Phys. Rev. Lett. 28, 292 (1972).
[34]C. K. Hall and G. Stell, Phys. Rev. A 7, 1679 (1973).
[35]R. Kikuchi, Phys. Rev. 81, 988 (1951).
[36]J. Hijmans and J. de Boer, Physica 21, 471 (1955).
[37]F. E. J. Kruseman Aretz and E. G. D. Cohen, Physica 26, 967 (1960).
[38]G. A. Cook, *Argon, Helium and the Rare Gases* (Interscience, New York, 1961), Vol. I.
[39]R. M. Nisbet and I. E. Farquhar, Phys. Rev. A 5, 380 (1972).
[40]W. K. Theumann and J. S. Høye, J. Chem. Phys. 55, 4159 (1971).
[41]J. F. Nagle and J. C. Bonner, J. Chem. Phys. 54, 729 (1971).
[42]G. Stell and P. C. Hemmer, J. Chem. Phys. 56, 4274 (1972).
[43]H. P. Neumann, Z. Naturforsch. 29a, 65 (1974).
[44]H. P. Neumann, J. Stat. Phys. 13, 2 (1975).
[45]H. P. Neumann, Phys. Rev. A 11, 1043 (1975).